EUROPEAN ORGANIZATION FOR NUCLEAR RESEARCH (CERN)

CMS-EWK-10-012

Jet Production Rates in Association with W and Z Bosons in pp Collisions at $\sqrt{s} = 7$ TeV

The CMS Collaboration*

Abstract

Measurements of jet production rates in association with W and Z bosons for jet transverse momenta above 30 GeV are reported, using a sample of proton-proton collision events recorded by CMS at $\sqrt{s} = 7$ TeV, corresponding to an integrated luminosity of 36 pb^{-1}. The study includes the measurement of the normalized inclusive rates of jets $\sigma(V+ \geq n$ jets$)/\sigma(V)$, where V represents either a W or a Z. In addition, the ratio of W to Z cross sections and the W charge asymmetry as a function of the number of associated jets are measured. A test of Berends–Giele scaling at $\sqrt{s} = 7$ TeV is also presented. The measurements provide a stringent test of perturbative-QCD calculations and are sensitive to the possible presence of new physics. The results are in agreement with the predictions of a simulation that uses explicit matrix element calculations for final states with jets.

Submitted to the Journal of High Energy Physics

*See Appendix A for the list of collaboration members

1 Introduction

The study of jet production in association with a W or Z vector boson (denoted by 'V' in this paper) provides a stringent test of perturbative QCD calculations. The presence of a vector boson provides a clear signature of the process and allows comparison of different scattering amplitudes with respect to inclusive multijet production, which is dominated by gluon scattering. In addition, a precise measurement of the W (Z) + n jets cross section is essential since the production of vector bosons with jets constitutes a background in searches for new physics and for studies of the top quark. At present, next-to-leading-order (NLO) predictions are available for V + n jets, with n up to four [1–5].

The W^+ to W^- cross-section ratio for an associated jet multiplicity is also predicted by the theory [6] and larger than unity. Deviations of this ratio from the expected value may point to new processes that produce W bosons in the final state.

The CDF, D0 and ATLAS Collaborations have reported measurements of W (Z) + n jets production in [7–11].

This paper presents results obtained with the 2010 data sample of the Compact Muon Solenoid (CMS) experiment at the Large Hadron Collider (LHC), based on an integrated luminosity of $35.9 \pm 1.4 \text{ pb}^{-1}$ [12], collected in proton-proton collisions at 7 TeV. To reduce systematic uncertainties associated with the integrated luminosity measurement, the jet energy scale (JES), the lepton reconstruction, and the trigger efficiencies, we measure the V + n jets cross sections relative to the inclusive W and Z cross sections, $\sigma(\text{V}+ \geq n \text{ jets})/\sigma(\text{V})$. A clear advantage of using ratios of cross sections is also that theoretical uncertainties tend to cancel, improving the robustness of the results. We also measure the ratio of the W to Z cross sections and the W charge asymmetry as a function of the associated jet multiplicity. Finally, we test the Berends–Giele scaling hypothesis [13]. To compare the measurements with the predictions of the theoretical calculations, the results are presented at "particle level", unfolding the detector efficiency and resolution.

2 The CMS Experiment

The central feature of the CMS apparatus is a superconducting solenoid of 6 m internal diameter, providing an axial magnetic field of 3.8 T. Within the field volume are a silicon pixel and strip tracker, an electromagnetic calorimeter (ECAL), and a brass/scintillator hadron calorimeter (HCAL). Muons are detected in gas-ionization detectors embedded in the steel return yoke.

A right-handed coordinate system is used in CMS, with the origin at the nominal interaction point, the x-axis pointing to the centre of the LHC ring, the y-axis pointing up (perpendicular to the LHC plane), and the z-axis along the anticlockwise-beam direction. The polar angle θ is measured from the positive z-axis and the azimuthal angle ϕ is measured from the positive x-axis in the x-y plane. The pseudorapidity is defined as $\eta = -\ln[\tan(\theta/2)]$.

The inner tracker contains 1440 silicon pixel and 15148 silicon strip detector modules. It measures charged particle trajectories in the pseudorapidity range $|\eta| \leq 2.5$. The ECAL consists of nearly 76000 lead tungstate crystals that provide coverage for $|\eta| \leq 1.479$ in a cylindrical barrel region (EB) and $1.479 \leq |\eta| \leq 3.0$ in the two endcap regions (EE). Preshower detectors, each consisting of two planes of silicon sensors interleaved with a total of 3 radiation length of lead, are located in front of both EEs. The HCAL is a sampling device with brass as the passive material and scintillator as the active material. The combined calorimeter cells are

grouped in projective towers of granularity $\Delta\eta \times \Delta\phi = 0.087 \times 0.087$ at central rapidities and $\Delta\eta \times \Delta\phi \approx 0.17 \times 0.17$ at forward rapidities. Muons are detected in the pseudorapidity range $|\eta| \leq 2.4$, with detection planes based on three technologies: drift tubes, cathode strip chambers, and resistive plate chambers. In addition to the barrel and endcap detectors, CMS has extensive forward calorimetry. The first level (L1) of the trigger system, composed of custom hardware processors, is designed to select event candidates in less than 3.2 μs using information from the calorimeters and muon detectors. The high level trigger (HLT) processor farm further reduces the event rate to a few hundred hertz, before data storage. A more detailed description of CMS can be found elsewhere [14].

3 Data and Simulation Samples

The L1 trigger system selected electrons with an energy deposit in the ECAL of at least 5 GeV or 8 GeV, depending on the luminosity conditions, and muons with a transverse momentum exceeding 7 GeV. The events were then filtered by the HLT with algorithms that evolved in response to the rapid rise of the LHC luminosity during 2010. The p_T threshold of the electrons and muons was adjusted periodically, to cope with the increasing instantaneous luminosity. The largest sample of electrons was collected with an online requirement $p_T \geq 17$ GeV. For muons, most data were collected with a threshold of $p_T \geq 15$ GeV.

Simulated Monte Carlo (MC) samples are used for data/simulation comparison and to unfold the jet multiplicity distributions. Backgrounds are estimated from data, as explained below.

Samples of simulated events with a W or a Z boson are generated with the MADGRAPH 4.4.13 [15] event generator, interfaced to the PYTHIA 6.422 [16] program for parton shower simulation. The set of parton distribution functions used is CTEQ6L1 [17]. The MADGRAPH generator produces parton-level events with a vector boson and up to four partons on the basis of a matrix-element calculation. This sample serves as the baseline for comparisons with data. Additional samples of W and Z events are generated with PYTHIA. For jet multiplicities greater than one, MADGRAPH is expected to be more accurate since it uses the exact matrix-element calculation, while in PYTHIA only the hardest emission reproduces the exact matrix-element calculation. Top-pair (t$\bar{\text{t}}$) and single-top production processes are generated with MADGRAPH. Processes of multijet, γ+jets, b-hadron and c-hadron decays to final states with electrons and muons are generated with PYTHIA.

The full list of simulated samples is given in Table 1. In order to compare with the data distributions, the simulation samples are normalized to the cross sections times the integrated luminosity, using or NLO or next-to-next-to-leading-order (NNLO) cross sections [18–20], or the leading-order (LO) cross sections from the MC generator, as reported in the table.

Generated events are processed through a full detector simulation program based on GEANT4 [21, 22], followed by a detailed emulation of the trigger and event reconstruction. Minimum-bias events are superimposed on the generated events to reproduce the distribution of multiple proton-proton collisions in the same bunch crossing (pileup) observed in 2010. A signal sample without pileup is used for purpose of comparison. The PYTHIA parameters for the underlying event are set to the Z2 tune [23], which is a modification of the Z1 tune described in Ref. [24]. Comparisons are also made to the D6T tune [25].

Table 1: Summary of simulated datasets for the various signal and background processes used in this analysis. The requirements applied to leptons p_T and η, dilepton invariant mass ($M_{\ell\ell}$), and transverse momentum of the hard interaction ($\hat{p}_T$), are shown, and the corresponding cross section is given.

Process	Generator	Kinematic selection	σ (pb)
$W \to \ell\nu$	MADGRAPH	no selection	3.1×10^4 (NNLO)
$Z \to \ell^+\ell^-$	MADGRAPH	$M_{\ell\ell} > 50$ GeV	3.0×10^3 (NNLO)
$t\bar{t}$	MADGRAPH	no selection	1.6×10^2 (NLO)
Single-top tW channel	MADGRAPH	no selection	1.1×10^1 (LO)
Single-top s and t channels	MADGRAPH	no selection	3.5 (NLO)
$W \to e\nu$	PYTHIA	$|\eta_e| < 2.7$	8.2×10^3 (NNLO)
$W \to \mu\nu$	PYTHIA	$|\eta_\mu| < 2.5$	7.7×10^3 (NNLO)
$W \to \tau\nu$	PYTHIA	no selection	1.0×10^4 (NNLO)
$Z \to \ell^+\ell^-$	PYTHIA	$M_{\ell\ell} > 20$ GeV	5.0×10^3 (NNLO)
Inclusive μ QCD multijet	PYTHIA	$\hat{p}_T > 20$ GeV, $p_T^\mu > 10$ GeV, $|\eta_\mu| < 2.5$	3.4×10^5 (LO)
EM-enriched QCD multijet	PYTHIA	20 GeV $< \hat{p}_T < 170$ GeV	5.4×10^6 (LO)
$b/c \to e$	PYTHIA	20 GeV $< \hat{p}_T < 170$ GeV	2.6×10^5 (LO)
γ+jet	PYTHIA	no selection	8.5×10^7 (LO)

4 Signal Selection

Signal selection begins with the identification of a charged lepton, either an electron or a muon, with $p_T > 20$ GeV. This lepton, which will be called the "leading lepton", must geometrically match the object that triggered the event readout.

For electron candidates, we require that the ECAL cluster lies in the fiducial region $|\eta| < 2.5$, with the exclusion of the region $1.4442 < |\eta| < 1.566$. This exclusion allows us to reject electrons close to the barrel/endcap transition and electrons in the first endcap trigger tower, which lies in the shadow of cables and services. A series of quality requirements, following the standard established by the measurement of the inclusive W and Z cross sections [26], are then applied to the electron, as briefly described below.

For each electron candidate, a supercluster in ECAL is defined in order to correct for the potential underestimation of the energy due to bremsstrahlung. Thus the electron cluster is combined with the group of single clusters attributed to bremsstrahlung photons generated in the material of the tracker. Electrons are first selected based on the spatial matching between the ECAL supercluster and the silicon detector track in the η and ϕ coordinates, on the supercluster energy distribution in the η direction, and on the energy leakage into the HCAL detector. To reduce the contamination from converted photons, a minimal track transverse impact parameter significance is required. Electrons are rejected if no associated track hits are found in the first tracker layers or if a conversion partner candidate is found.

To reduce further the contamination from misidentified electrons and hadronic decays, we select electrons isolated from hadronic activity. This selection is based on maximum values allowed for three isolation variables. The variables are computed relative to the electron E_T and consist of the sums of track p_T in the tracker, energy deposits in ECAL, and energy deposits in HCAL, respectively. The sums are computed inside the cone $\Delta R = \sqrt{(\Delta\eta)^2 + (\Delta\phi)^2} < 0.3$, where $\Delta\eta$ and $\Delta\phi$ are the differences in the pseudorapidity and azimuthal angle between the electron and the track or energy deposit, with an inner exclusion region that removes the electron contribution.

For the leading electron, the values of the different quality requirements are chosen such that

they correspond to a lepton efficiency of about 80%, as evaluated with the MADGRAPH +PYTHIA simulated sample described in Section 6.

After identifying the leading electron, we search for a second electron candidate called the "second leading electron", within the ECAL fiducial volume and with $p_T > 10$ GeV. The quality requirements for the second leading electron are tuned to provide an electron efficiency of about 95%, as evaluated with the MADGRAPH +PYTHIA simulated sample. If such a second leading electron is found, and its invariant mass with the first leading electron $M_{\ell\ell}$ lies between 60 GeV and 120 GeV, the event is assigned to the Z + jets sample. If such a second leading electron is not found, the event is assigned to the W + jets sample, thereby ensuring that there is no overlap between the two samples. Events including a muon with $p_T > 15$ GeV and $|\eta| < 2.4$ are rejected from the W + jets electron sample to reduce $t\bar{t}$ contamination.

The muon reconstruction and identification are identical to that used for the measurement of the W and Z cross sections [26]. A relative isolation variable, $I = \sum(p_T^{\text{track}} + E_T^{\text{HCAL}} + E_T^{\text{ECAL}})/p_T^{\mu}$ is defined, which includes the p_T for tracks, ECAL, and HCAL towers in a cone $\Delta R < 0.3$ around the muon direction. The muon and its energy deposits are excluded from the sum. A muon is considered to be isolated if $I < 0.15$. The V + jets muon event selection starts by requiring the presence of an isolated muon in the region $|\eta| < 2.1$ with $p_T > 20$ GeV. It must be a high-quality muon as described in [26] with an impact parameter in the transverse plane $|d_{xy}| < 2$ mm, to suppress cosmic-ray background. As for the electron channel, we then search for a second leading muon with $p_T > 10$ GeV and $|\eta| < 2.4$, such that the dimuon invariant mass lies between 60 GeV to 120 GeV. If such a second leading muon is (is not) found, the event is assigned to the Z + jets (W + jets) sample. An electron veto is not applied in the selection of W decays into muons as it would significantly lower the efficiency and increase the systematic uncertainty, because of fake electrons.

For the W + jets samples in both decay modes, we compute the missing transverse energy $\slashed{E}_T$ using a particle-flow (PF) algorithm [27] that reconstructs individually each particle in the event based on information from all relevant subdetectors. We then use it to calculate the transverse mass, $M_T = \sqrt{2p_T\slashed{E}_T(1 - \cos\Delta\phi)}$, where $\Delta\phi$ is the angle in the x-y plane between the directions of the lepton p_T and the $\slashed{E}_T$, and select events with $M_T > 20$ GeV.

For the charge asymmetry measurement, the charge assignment of the lepton is used to select $W^+ + $ jets and $W^- + $ jets candidates. For electrons, three algorithms are used to determine their charge [28]: the curvature of the electron track reconstructed by a Gaussian-sum-filter algorithm [29], the curvature of the silicon detector track associated with the electron, and the difference in ϕ between the track direction at the interaction vertex and the supercluster measured by the ECAL. In order to reduce uncertainties related to charge misassignment, we reject the event if the charge value differs amongst the three methods.

5 Jet Rates

Jets are reconstructed from the particle collection created with the particle-flow algorithm and are formed with the anti-k_T clustering algorithm [30] with a size parameter of $R = 0.5$. Jet energy corrections (JEC) are applied to account for the jet energy response as a function of η and E_T [31].

We require the jet to have $|\eta| < 2.4$ to be in the tracker acceptance, and $E_T > 30$ GeV. Jets are required to satisfy identification criteria that eliminate jets originating from or seeded by noisy channels in the hadron calorimeter [32].

The pileup and the underlying event affect the jet counting by contributing additional energy to the measured jet energy and therefore "promoting" jets above the E_T threshold for jet counting. To minimize the uncertainty due to pileup and the underlying event, the E_T threshold is set at 30 GeV. The average number of pileup events in the data sample is 2.7. Their effect is taken into account by evaluating event-by-event the energy not related to the hard-interaction activity [33, 34]. This amount is subtracted from each jet [31]. Removing the average energy due to pileup does not remove the jets from pileup interactions. In a simulated sample, this additional contribution to the jet count, however, is found to be negligible for the chosen jet E_T threshold.

Electrons can be reconstructed as jets or can overlap with a jet. Therefore, jets that fall within $\Delta R < 0.3$ of an electron from W or Z decay are not included in the jet count. Muons can also overlap with a jet, thus, each selected muon is matched to one of the particles reconstructed by the PF algorithm and excluded from jet clustering.

One of the most important backgrounds in the W sample at high jet multiplicity comes from $t\bar{t}$ events. These contain two b-quark jets. We count the number of b-tagged jets, $n_{\text{jet}}^{\text{b-tagged}}$, with a tagging algorithm that requires at least two tracks in the jet with a significance on the transverse impact parameter greater than 3.3. The algorithm parameters chosen correspond to a working point with an efficiency of about 62% and a mistag rate of about 2.9%. The efficiency is measured from data using a sample of $t\bar{t}$ events with fully leptonic final states. The mistag rate is averaged over light jets in simulated W and top events, and corrected for measured differences between data and simulation [35]. The $n_{\text{jet}}^{\text{b-tagged}}$ value is then used in the fitting method to extract the number of signal events, as described in Section 7.

The observed transverse energy distributions of the leading jet in the $W+ \geq 1$ jet and $Z+ \geq 1$ jet samples are shown in Figs. 1 and 2, respectively. Figures 3 and 4 show the same distributions for the second-leading jet in the $W+ \geq 2$ jets and $Z+ \geq 2$ jets samples. In addition to the selection described in Section 4, for the transverse energy distributions, W boson candidate are required to have $M_T > 50$ GeV, thus reducing significantly the QCD multijet contamination. The $t\bar{t}$ background is larger in the muon than in the electron channel because an electron veto is not applied, as explained in Section 4. The data are in good agreement with the MADGRAPH + PYTHIA parton shower predictions normalized to the NNLO cross sections.

The selected events are assigned to bins of jet multiplicity by counting the number of jets with $E_T > 30$ GeV. The number of events with a W (Z) candidate and at least one jet are 43561 (1648) in the electron channel, and 32496 (2339) in the muon channel. The observed distributions of the exclusive numbers of reconstructed jets in the W and Z samples are shown in Figs. 5 and 6, respectively. The distributions from simulation are also shown. They are normalized to the integrated luminosity using the cross-section values in Table 1. Comparisons between the data and simulation distributions show that there is a very good agreement, even prior to any attempt to fit the signal and background content of the data. For the W sample, QCD multijet processes constitute the most significant source of background in the lower jet-multiplicity bins, while top quark production dominate in the higher jet-multiplicity bins. For Z events with one or more jets, the top quark production dominates the background, which overall is very small.

6 Acceptance and Efficiency

In order to provide model-independent results, we do not correct for the detector acceptance, but rather quote the results within the acceptance, as defined by the lepton and jet fiducial and kinematic selections given above.
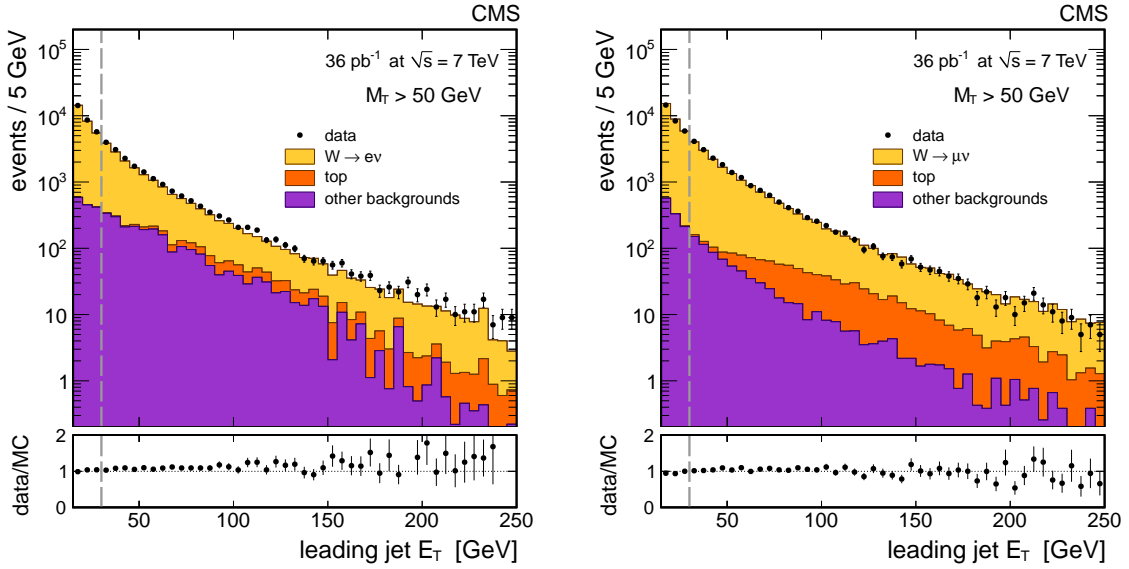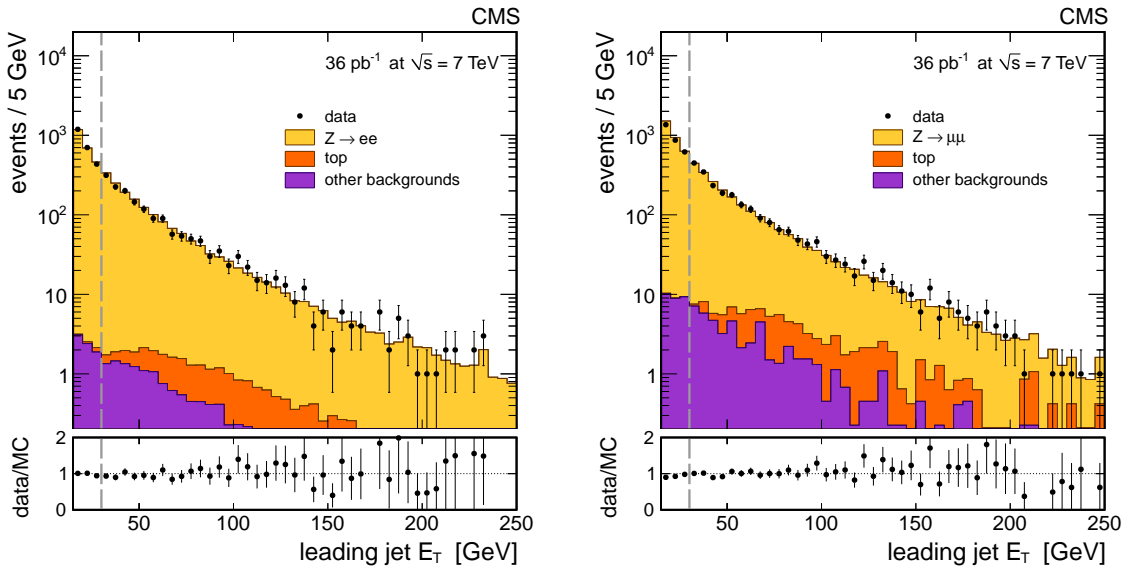
Figure 1: Distributions of the E_T for the leading jet in the $W+ \geq 1$ jet sample for the electron channel (left) and for the muon channel (right), before the requirement of $E_T > 30$ GeV (shown by the vertical dotted line) is imposed for counting jets. Points with error bars are data, histograms represent simulation of the signal (yellow), $t\bar{t}$ and single top backgrounds (orange) and other backgrounds (purple). The last includes multijet events, Z events, and events in which the W decays to a channel other than the signal channel. Error bars represent the statistical uncertainty on the data. The ratio between the data and the simulation is shown in the lower plots.
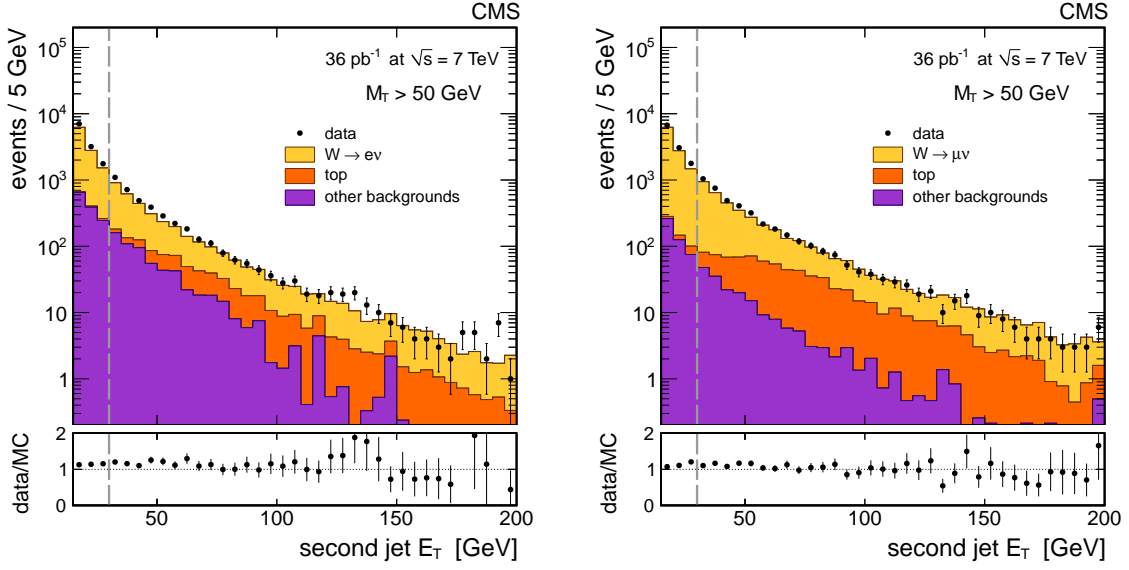

Figure 2: Distributions of the E_T for the leading jet in the $Z+ \geq 1$ jet sample for the electron channel (left) and for the muon channel (right), before the requirement of $E_T > 30$ GeV (shown by the vertical dotted line) is imposed for counting jets. Points with error bars are data, histograms represent simulation of the signal (yellow), $t\bar{t}$ and single top backgrounds (orange) and other backgrounds (purple). The last includes multijet events, W events, and events in which the Z decays to a channel other than the signal channel. Error bars represent the statistical uncertainty on the data. The ratio between the data and the simulation is shown in the lower plots.

Figure 3: Distributions of the E_T for the second leading jet in the W+ $\geq$ 2 jets sample for the electron channel (left) and for the muon channel (right), before the requirement of $E_T > 30$ GeV (shown by the vertical dotted line) is imposed for counting jets. Points with error bars are data, histograms represent simulation of the signal (yellow), $t\bar{t}$ and single top backgrounds (orange) and other backgrounds (purple). The last includes multijet events, Z events, and events in which the W decays to a channel other than the signal channel. Error bars represent the statistical uncertainty on the data. The ratio between the data and the simulation is shown in the lower plots.
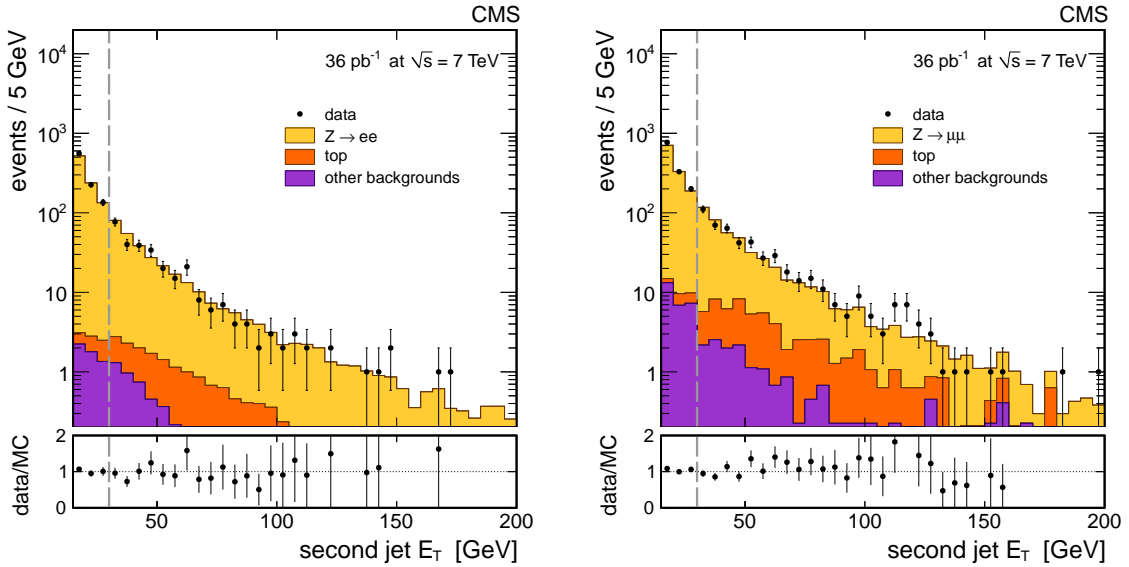

Figure 4: Distributions of the E_T for the second leading jet in the Z+ $\geq$ 2 jets sample for the electron channel (left) and for the muon channel (right), before the requirement of $E_T > 30$ GeV (shown by the vertical dotted line) is imposed for counting jets. Points with error bars are data, histograms represent simulation of the signal (yellow), $t\bar{t}$ and single top backgrounds (orange) and other backgrounds (purple). The last includes multijet events, W events, and events in which the Z decays to a channel other than the signal channel. Error bars represent the statistical uncertainty on the data. The ratio between the data and the simulation is shown in the lower plots.
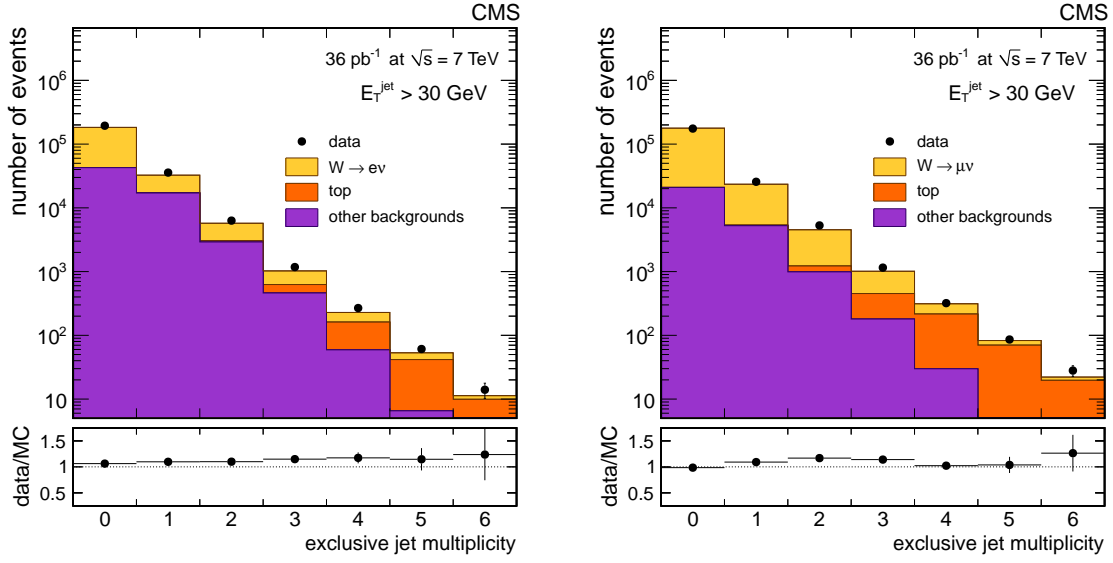
Figure 5: Exclusive number of reconstructed jets in events with $W \to e\nu$ (left) and $W \to \mu\nu$ (right). Points with error bars are data, histograms represent simulation of the signal (yellow), $t\bar{t}$ and single top backgrounds (orange) and other backgrounds (purple). Error bars represent the statistical uncertainty on the data. These distributions have not been corrected for detector effects or selection efficiency. The ratio between the data and the simulation is shown in the lower plots.
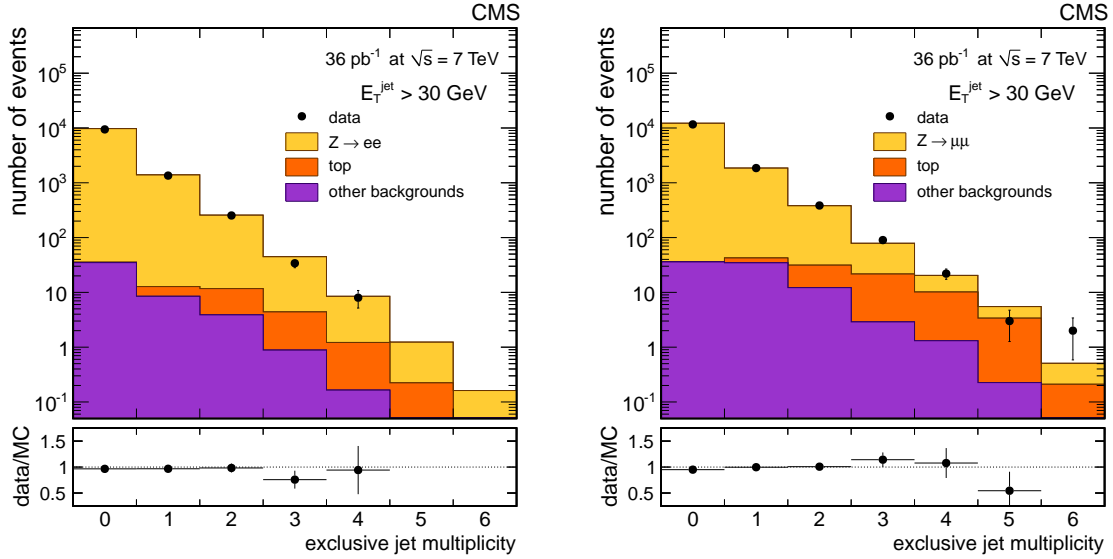

Figure 6: Exclusive number of reconstructed jets in events with $Z \to e^+e^-$ (left) and $Z \to \mu^+\mu^-$ (right). Points with error bars are data, histograms represent simulation of the signal (yellow), $t\bar{t}$ and single top backgrounds (orange) and other backgrounds (purple). Error bars represent the statistical uncertainty on the data. These distributions have not been corrected for detector effects or selection efficiency. The ratio between the data and the simulation is shown in the lower plots.

The efficiencies for lepton reconstruction, identification, isolation, and trigger are obtained from $Z + \text{jets}$ data samples. The sample for the measurement of a given efficiency contains events selected with two lepton candidates. One lepton candidate, called the "tag", satisfies all selection requirements, including the matching to a trigger object. The other lepton candidate, called the "probe", is selected with criteria that depend on the efficiency being measured. The invariant mass of the tag and probe lepton candidates must fall in the range [60–120] GeV. The signal yields are obtained for two exclusive subsamples of events in which the probe lepton passes or fails the selection criteria considered. Fits are performed to the invariant-mass distributions of the "pass" and "fail" subsamples, including a term that accounts for the background. The measured efficiency is deduced from the relative levels of signal in the "pass" and "fail" subsamples. An estimate of the systematic uncertainty on the efficiency is obtained by varying the shape used to fit the Z signal among several functional forms tested on the simulation. The lepton selection efficiency is the product of three components: the reconstruction efficiency, the identification and isolation efficiency, and the trigger efficiency. Each of these efficiencies is calculated as a function of the jet multiplicity in the event. The efficiency of additional selection requirements applied to W events is computed from the simulation.

For electrons we find that the efficiency is about 70% (60%) for the $W + \text{jets}$ ($Z + \text{jets}$) signal events with variations of a few percent across different jet multiplicity bins, which are accounted for in the measurement. The uncertainty ranges from about 1% up to about 5%, increasing with the number of jets in the event. The additional requirement that the three methods to measure the electron charge agree, which is applied for the charge asymmetry measurement, has an efficiency of 97%.

For muons, the efficiencies are measured as a function of p_{T}, η and the jet multiplicity. The efficiency dependence on p_{T} and η is measured in events with zero and one jet. For events with more than one jet, where the sample size is insufficient for a (p_{T}, η) dependent efficiency to be measured, an average efficiency is computed and the (p_{T}, η) dependence measured in the $n = 1$ bin is assumed. The isolation efficiency is found to have the largest dependence on multiplicity, while the trigger, reconstruction, and identification efficiencies are consistent with being constant. The average efficiency is 85% and 86% for W and Z events, respectively. They are similar because the efficiency for selecting the second muon from Z candidates and for passing the M_{T} criteria with W candidates are both near unity. While the second muon efficiency in Z events is fairly flat across different jet multiplicity bins, the efficiency of the M_{T} requirement for W candidates decreases to 90% for high jet multiplicity. The uncertainty on the muon efficiency ranges from about 3% up to about 15%, increasing with the number of jets in the event.

Electron charge misidentification is estimated with simulated samples and data. It depends on the lepton η, with the largest misidentification in the endcap regions. The probability ranges from 4×10^{-4} up to 3×10^{-3} in the simulation, and from 1×10^{-3} up to 4×10^{-3} in the data. The difference between simulation and data is taken as uncertainty. The muon charge misidentification has been found to be smaller than 10^{-4} in cosmic-ray data [36], therefore yielding a negligible systematic uncertainty. Using the tag-and-probe method, the ratio of the selection efficiency for electrons to positrons is measured to equal unity within the statistical precision of 1.4% [28]. The efficiency ratio between μ^{+} and μ^{-} is found equal to one within 2% [28]. Effects related to charge measurements are propagated as systematic uncertainties to the final W charge asymmetry results.
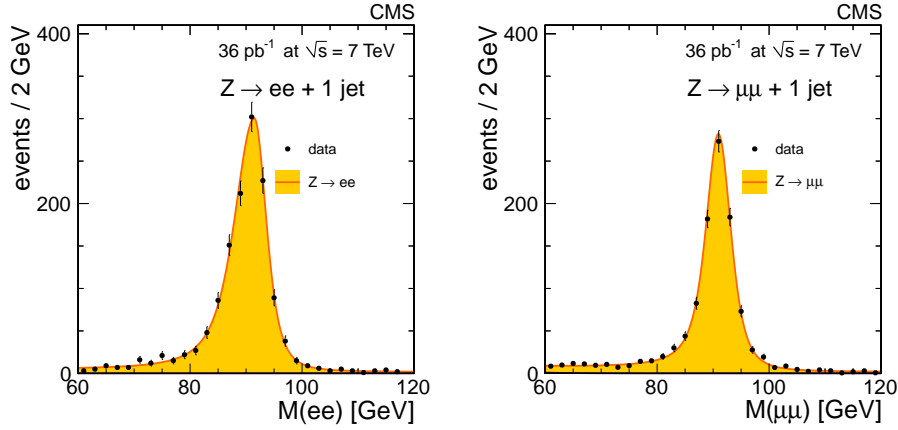
Figure 7: Dilepton mass for the $Z + 1$ jet samples, in the electron channel (left) and the muon channel (right). Points with error bars are data. The fit result for the signal is shown by the yellow-filled area. The background is too small to be visible in the figure.

7   Signal Extraction

The signal yield is estimated using an extended maximum-likelihood fit to the dilepton invariant mass ($M_{\ell\ell}$) distribution for the $Z +$ jets sample, and to the transverse mass (M_T) distribution for the $W +$ jets sample; the number of observed events is included in the likelihood fit as a constraint on the normalization. The probability distribution functions are asymmetric Gaussians with tails. Their parameters are derived from the simulation or, for the background, from control data samples with inverted identification (isolation) requirement on the electrons (muons).

For the Z event sample, the contamination from the background processes, dominated by $t\bar{t}$ and $W +$ jets, is small and does not produce a peak in the $M_{\ell\ell}$ distributions, so the $M_{\ell\ell}$ distribution is taken to be the sum of two components, one for the signal and one that accounts for all background processes.

For the W sample, the background contributions can be divided into two components, one which exhibits a peaking structure in M_T, dominated by $t\bar{t}$, and another which does not, dominated by QCD multijet events. We perform a two-dimensional fit to the M_T distribution and the number of b-tagged jets, $n_{\text{jet}}^{\text{b-tagged}}$. The M_T distribution allows the statistical separation of the signal from the non-peaking backgrounds, while $n_{\text{jet}}^{\text{b-tagged}}$ distinguishes the signal and the background from $t\bar{t}$. The likelihood function is built under the assumption that there are no b jets in the signal events. This implies that a fraction of W events produced in association with heavy-flavour jets, i.e. the fraction with at least one heavy-flavour jet in the acceptance, is counted as background. Considering the statistical precision of the measurement, this assumption has a negligible effect on the $W +$ jets cross-section result.

The fits are done using the jet multiplicity bins for $n \leq 3$; in contrast, the jet counting is done inclusively for the last bin of jet multiplicity, i.e. $n \geq 4$. Examples of fits for $Z + 1$ jet are shown in Fig. 7. Figures 8 and 9 show fits in M_T and $n_{\text{jet}}^{\text{b-tagged}}$ projections for the $W + n$ jets (n=1 and n=3) channel. The presence of the top quark background is evident from comparing the $n = 1$ and $n = 3$ multiplicity bins. The fit is repeated separately on the $W^+ +$ jets and $W^- +$ jets samples for the charge-asymmetry measurement.

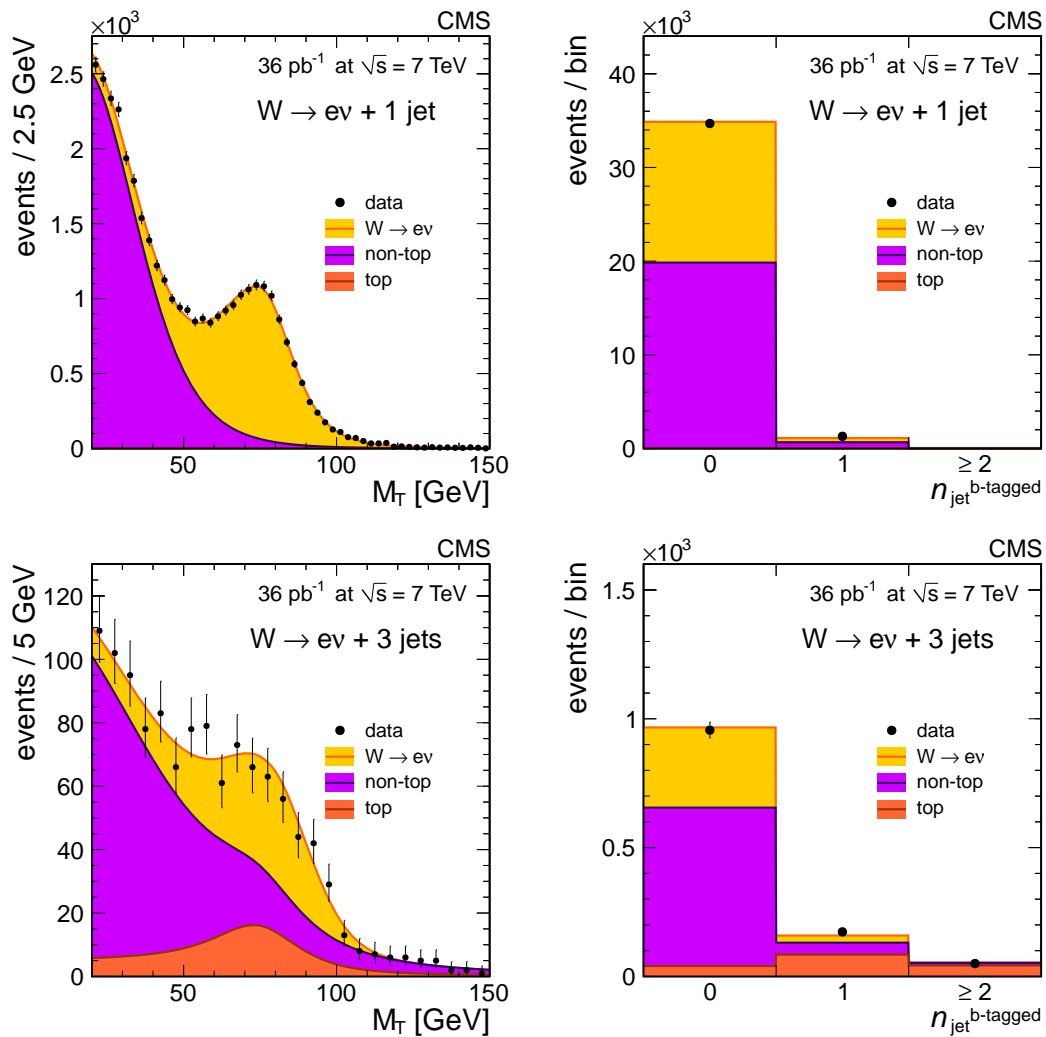In the electron channel, the observed exclusive V + jets yields determined from the fit are cor-

Figure 8: Fit results for the W($e\nu$) + n jets sample with $n = 1$ (upper row) and $n = 3$ (lower row). For each row, the M_T projection is shown on the left, while the $n_{\text{jet}}^{\text{b-tagged}}$ projection is shown on the right. Points with error bars are data. Fit results are shown by the colour-filled areas for the signal process (yellow), non-top backgrounds (purple), and top backgrounds (orange).
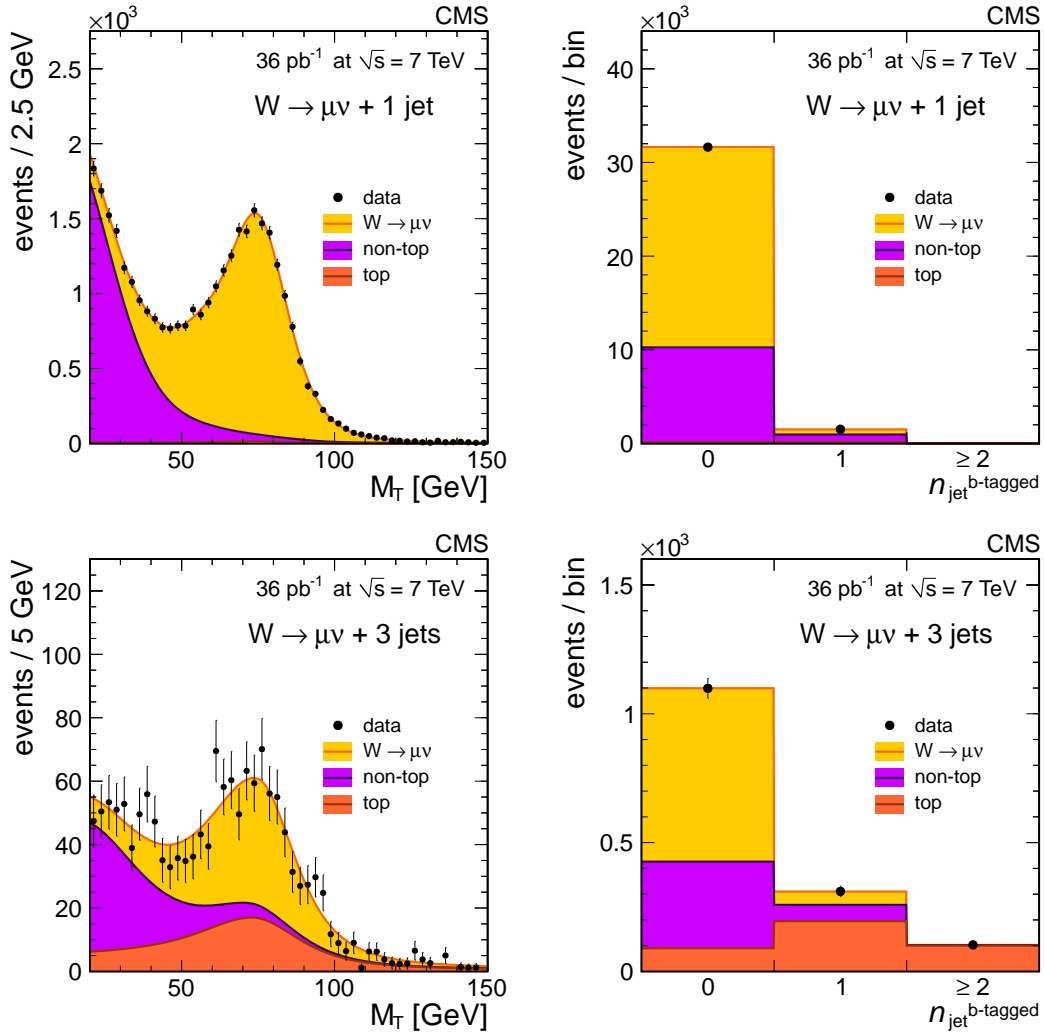
Figure 9: Fit results for the $W(\mu\nu) + n$ jets sample with $n = 1$ (upper row) and $n = 3$ (lower row). For each row, the M_T projection is shown on the left, while the $n_{\text{jet}}^{\text{b-tagged}}$ projection is shown on the right. Points with error bars are data. Fit results are shown by the colour-filled areas for the signal process (yellow), non-top backgrounds (purple), and top backgrounds (orange).

rected a posteriori for electron efficiencies, which are discussed in Section 6. In the muon channel, efficiencies are available in bins of the lepton p_T, η and the jet multiplicity. This allows an efficiency-weighted fit to be performed, which returns efficiency-corrected yields.

8 Unfolding

In order to estimate the scaling behaviour of the jets at the particle-jet level, we apply an unfolding procedure that removes the effects of jet energy resolution and reconstruction efficiency. The migration matrix, which relates a number n' of produced jets at the particle level to an observed number n of reconstructed jets, is derived from simulated samples of $Z + jets$ and $W + jets$. The unfolding procedure takes into account the statistical and systematic uncertainties in the signal yields.

The migration matrices are derived from simulated events with leptons and jets within the p_T and η acceptance of the analysis. The simulation is performed using the MADGRAPH generator with the Z2 tune and incorporates event pileup.

Two unfolding methods are employed. The baseline method is the "singular value decomposition" (SVD) algorithm [37]. As a crosscheck, the iterative method [38] is also applied. Both algorithms require a regularization parameter to prevent the statistical fluctuations in the data from appearing as structure in the unfolded distribution. For the SVD method, the regularization parameter is chosen to be $k_{\text{SVD}} = 5$, corresponding to the number of bins. This algorithm corresponds to an inversion of the migration matrix, and gives the most accurate uncertainty estimate. For the iterative algorithm, the regularization parameter $k_{\text{Bayes}} = 4$ is used, as suggested in Ref. [39].

9 Systematic Uncertainties

One of the dominant sources of systematic uncertainties in the V+jets measurements is the determination of the jet energy, which affects the jet counting. We consider three sources of uncertainty related to the jet energy scale:

- Corrections applied to the measured jet energy to account for the detector response and inhomogeneities. The corrections are derived from measured jet p_T in dijet and photon+jet events and are available as a function of η and p_T [31].

- The dependence of the detector response on the jet flavour. The difference between the flavour composition of jets in V+jets events and the flavour composition of the jet sample used to extract the corrections is accounted for by an additional 2% uncertainty on the jet energy.

- The average energy removed by the pileup subtraction method includes the activity due to the underlying event. We find that the jet energy is systematically decreased by 500 MeV in comparison with events without pileup. This amount is included as a systematic uncertainty on the jet energy.

The above uncertainties on the jet energy are added in quadrature and their effect is evaluated on the jet multiplicity distribution using simulation. Similar results are found in all the channels, for both W and Z events. For W events, the effect of the mismeasured jet energy on M_T is evaluated in the fitting procedure.

Uncertainty on the jet energy resolution also affects the jet multiplicity. The resolution is underestimated in the simulation by $(10 \pm 10)\%$ [40]. The effect of this uncertainty on the jet

multiplicity has been studied in simulated W + jets events and found to be below 2%.

The pileup subtraction method was tested by comparing the jet multiplicity in two simulated signal samples, one with pileup and one without, with the pileup subtraction applied in the former case. The difference, due to residual effects and jets in pileup events, is below 5%.

All the above uncertainties are added in quadrature and the resultant contribution to the relative systematic uncertainty on jet rates is shown in Tables 2 and 3. Also shown in these tables are the uncertainties associated with the selection efficiency and the signal extraction procedure. The largest source of uncertainty related to signal extraction in W events comes from the uncertainty of the b-tagging efficiency and mistag rates. This uncertainty is estimated with a control sample of $t\bar{t}$ events decaying into $e^{\pm}\mu^{\mp}$ and a pair of b jets. The uncertainty due to the selection efficiency in Tables 2 and 3 includes the uncertainty on the lepton efficiency and on the selection procedure. As discussed in Section 6, it is evaluated with Z + jets data samples, with different strategies for the electron and muon channels. This difference results in a larger systematic uncertainty on the muon channel. While the systematic uncertainty on the energy scale is correlated among the different jet multiplicities, all other uncertainties are not. The relative statistical uncertainty is also shown.

All statistical and systematic uncertainties are propagated in the unfolding procedure. Uncertainties due to the unfolding procedure itself are calculated as the differences between the unfolded rates using the SVD and the iterative algorithms, and the MADGRAPH, PYTHIA, and Z2 or D6T tunes of MADGRAPH for the unfolding matrix. The resulting uncertainties are shown with the final results in the next section.

10   Results

Results are given for the leptons within the acceptance defined by the kinematical selection cuts in the electron (muon) channels: leading-lepton $p_T > 20$ GeV and $|\eta| < 2.5$ (2.1); second-lepton $p_T > 10$ GeV and $|\eta| < 2.5$ (2.4). In addition, electrons in the $1.4442 < |\eta| < 1.566$ region are excluded, and jets are not counted if $\Delta R < 0.3$ with respect to an electron from the W or the Z. Since the acceptance is different, we do not combine the results for the electron and muon channels.

Two sets of ratios from the unfolded jet multiplicity distributions are calculated The first set of ratios is $\sigma(V+ \geq n \text{ jets})/\sigma(V)$, where $\sigma(V)$ is the inclusive cross section, and is presented in Tables 4 and 5 and in the upper frames of Figs. 10–13. The second set of ratios is $\sigma(V+ \geq n \text{ jets})/\sigma(V+ \geq (n-1) \text{ jets})$, reported in Tables 6 and 7 and in the lower frames of Figs. 10–13. The contributions of the systematic uncertainties associated with the jet energy scale (including pileup effects) and the unfolding are given in the tables and shown as error bands in the figures. For $n \geq 2$ jets, the PYTHIA pure parton shower simulation fails to describe the data, while the MADGRAPH simulation agrees well with the experimental spectrum. Because of the jet threshold $E_T > 30$ GeV, the sensitivity to the tuning of the underlying event is negligible. The expectations from the simulation with the Z2 and the D6T tunes are identical. Thus, in the rest of the paper we will only consider the Z2 tune for comparison with the data.

The statistical uncertainty quoted in the third column of Tables 4–7 includes only the statistical contribution from the fit results. It is combined (fourth column) with the systematic uncertainties from the fit and the statistical and systematic uncertainty on the efficiency, which are uncorrelated between the samples with different numbers of jets. To estimate the jet energy scale uncertainty, jet rates from the fits were scaled higher and lower according to this uncer-

tainty. Those numbers were then unfolded and the difference in the output from the actual fit value is quoted in the fifth column. Finally, the uncertainty due to the unfolding algorithm is evaluated as explained above and is shown in the last column of the tables.

The ratios of W + jets and Z + jets cross sections are shown in Fig. 14. Many important systematic uncertainties, such as those on integrated luminosity and jet energy scale, cancel in the ratio. The most significant remaining systematic uncertainty is due to the selection efficiency, which could be correlated between different bins because of the M_T cut in the W candidate

Table 2: Relative systematic and statistical uncertainties on the measured jet multiplicity in W events, as a function of the jet multiplicity for electron and muon samples.

Uncertainties on jet rate in W $\to$ eν events [%]					
Jet multiplicity	0	1	2	3	≥ 4
Energy scale and pileup	± 5	± 8	$^{+11}_{-10}$	$^{+14}_{-12}$	$^{+16}_{-15}$
Selection efficiency	± 0.5	± 0.3	± 1.0	± 1.7	± 4
Signal extraction		± 0.1	± 0.4	± 3	± 9
Total systematic uncertainty	± 5	± 8	$^{+11}_{-10}$	$^{+14}_{-12}$	± 17
Statistical uncertainty	± 0.3	± 1.0	± 2.4	± 10	± 28
Uncertainties on jet rate in W $\to$ $\mu\nu$ events [%]					
Jet multiplicity	0	1	2	3	≥ 4
Energy scale and pileup	± 5	± 8	$^{+11}_{-10}$	$^{+14}_{-12}$	$^{+16}_{-15}$
Selection efficiency	± 3	± 6	± 4	± 10	± 17
Signal extraction		± 0.1	± 0.4	± 3	± 9
Total systematic uncertainty	± 6	± 10	$^{+13}_{-12}$	$^{+19}_{-17}$	± 26
Statistical uncertainty	± 0.3	± 0.9	± 2.4	± 5.6	± 21

Table 3: Relative systematic and statistical uncertainties on the measured jet multiplicity rates in Z events, as a function of the jet multiplicity for electron and muon samples. The signal extraction uncertainty is not shown since it is negligible for Z events.

| Uncertainties on jet rate in Z $\to$ e$^+$e$^-$ events [%]					
Jet multiplicity	0	1	2	3	≥ 4
Energy scale and pileup	± 5	± 8	$^{+11}_{-10}$	$^{+14}_{-12}$	$^{+16}_{-15}$
Selection efficiency	± 1.1	± 1.0	± 2.2	± 2.6	± 6
Total systematic uncertainty	± 5	± 8	$^{+11}_{-10}$	$^{+14}_{-12}$	$^{+17}_{-16}$
Statistical uncertainty	± 1.1	± 3.1	± 7	± 17	± 43
Uncertainties on jet rate in Z $\to$ $\mu^+\mu^-$ events [%]					
Jet multiplicity	0	1	2	3	≥ 4
Energy scale and pileup	± 5	± 8	$^{+11}_{-10}$	$^{+14}_{-12}$	$^{+16}_{-15}$
Selection efficiency	± 3	$^{+6}_{-5}$	$^{+7}_{-6}$	± 10	$^{+24}_{-12}$
Total systematic uncertainty	± 6	± 10	$^{+13}_{-12}$	$^{+18}_{-16}$	$^{+30}_{-21}$
Statistical uncertainty	± 0.9	± 2.6	± 5.2	± 18	± 41
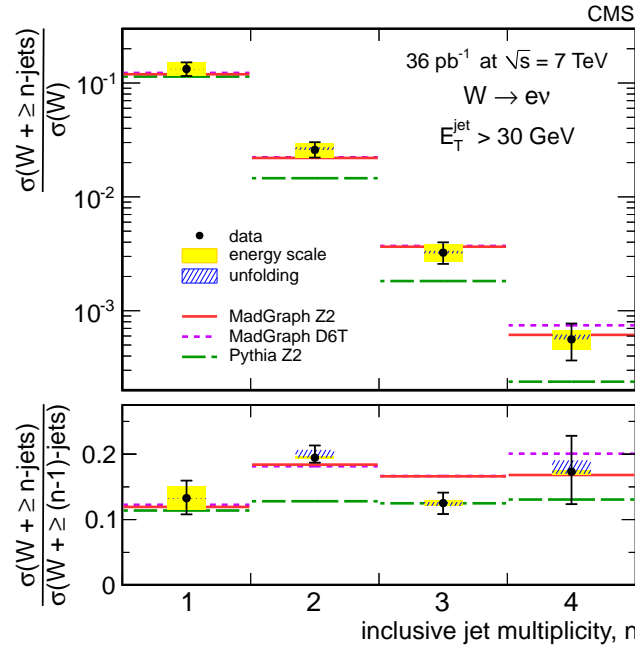
Figure 10: The ratios $\sigma(W+ \geq n \text{ jets})/\sigma(W)$ (top) and $\sigma(W+ \geq n \text{ jets})/\sigma(W+ \geq (n-1) \text{ jets})$ (bottom) in the electron channel compared with the expectations from two MADGRAPH tunes and PYTHIA. Points with error bars correspond to the data. The uncertainties due to the energy scale and unfolding procedure are shown as yellow and hatched bands, respectively. The error bars represent the total uncertainty.
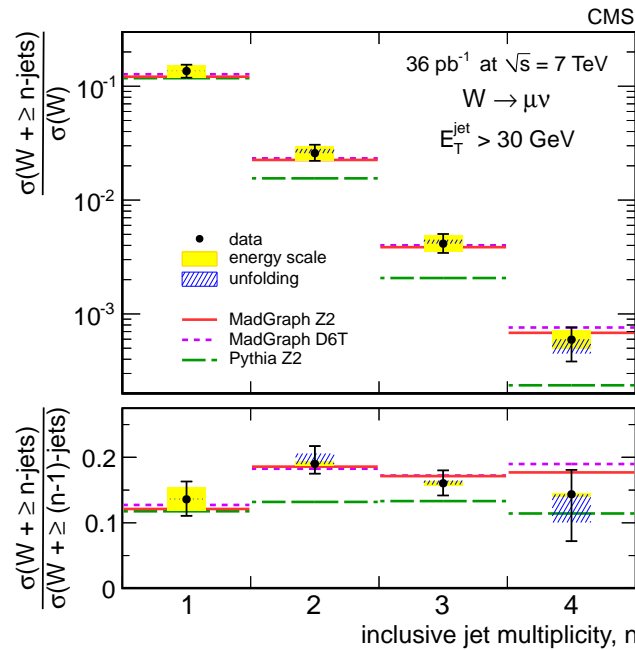

Figure 11: The ratio $\sigma(W+ \geq n \text{ jets})/\sigma(W)$ (top) and $\sigma(W+ \geq n \text{ jets})/\sigma(W+ \geq (n-1) \text{ jets})$ (bottom) in the muon channel compared with the expectations from two MADGRAPH tunes and PYTHIA. Points with error bars correspond to the data. The uncertainties due to the energy scale and unfolding procedure are shown as yellow and hatched bands, respectively. The error bars represent the total uncertainty.
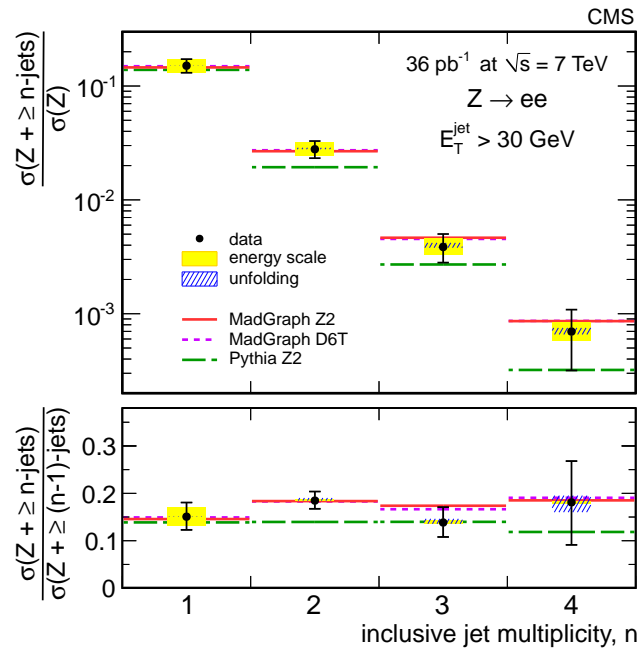
Figure 12: The ratio $\sigma(Z+ \geq n \text{ jets})/\sigma(Z)$ (top) and $\sigma(Z+ \geq n \text{ jets})/\sigma(Z+ \geq (n-1) \text{ jets})$ (bottom) in the electron channel compared with the expectations from two MADGRAPH tunes and PYTHIA. Points with error bars correspond to the data. The uncertainties due to the energy scale and unfolding procedure are shown as yellow and hatched bands, respectively. The error bars represent the total uncertainty.
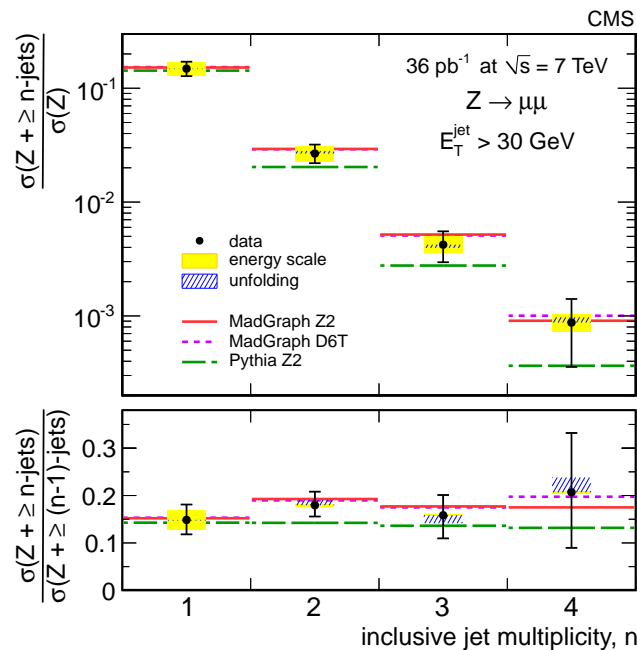

Figure 13: The ratio $\sigma(Z+ \geq n \text{ jets})/\sigma(Z)$ (top) and $\sigma(Z+ \geq n \text{ jets})/\sigma(Z+ \geq (n-1) \text{ jets})$ (bottom) in the muon channel compared with the expectations from two MADGRAPH tunes and PYTHIA. Points with error bars correspond to the data. The uncertainties due to the energy scale and unfolding procedure are shown as yellow and hatched bands, respectively. The error bars represent the total uncertainty.

selection. The maximal difference observed between the measured and expected values is at the level of one standard deviation, neglecting the uncertainties on the theoretical predictions. The difference between the expected value of the ratio in the electron and muon channels is due to the larger electron acceptance in η.

The charge asymmetry, defined as $A_{\mathrm{W}} = \frac{\sigma(W^+)-\sigma(W^-)}{\sigma(W^+)+\sigma(W^-)}$, is measured as a function of the number of jets in the events for the muon and electron channels, by fitting separately the events with positive and negative lepton charge. The sample size does not allow a measurement in events with four jets or more. Table 8 and Fig. 15 show the measured value of the charge asymmetry for the electron and muon events. The systematic uncertainties include those from the jet

Table 4: Results for $\sigma(W+ \geq n \text{ jets})/\sigma(W)$ in the electron and muon channels. A full description of the uncertainties is given in the text.

n jets	$\frac{\sigma(W+\geq n \text{ jets})}{\sigma(W)}$	stat.	stat. + efficiency and signal extraction	energy scale	unfolding
electron channel					
≥ 1 jets	0.133	0.002	0.002	$+0.019$ -0.017	± 0.001
≥ 2 jets	0.026	0.001	0.001	± 0.004	± 0.001
≥ 3 jets	0.0032	0.0004	0.0004	$+0.0006$ -0.0005	± 0.0001
≥ 4 jets	0.00056	0.00017	0.00018	$+0.00012$ -0.00010	$+0.00006$ -0.00001
muon channel					
≥ 1 jets	0.136	0.002	0.007	$+0.019$ -0.017	± 0.001
≥ 2 jets	0.026	0.001	0.002	± 0.004	$+0.002$ -0.001
≥ 3 jets	0.0041	0.0003	0.0005	$+0.0008$ -0.0006	$+0.0003$ -0.0001
≥ 4 jets	0.00059	0.00011	0.00017	$+0.00012$ -0.00010	$+0.00001$ -0.00015

Table 5: Results for $\sigma(Z+ \geq n \text{ jets})/\sigma(Z)$ in the electron and muon channels. A full description of the uncertainties is given in the text.

n jets	$\frac{\sigma(Z+\geq n \text{ jets})}{\sigma(Z)}$	stat.	stat. + efficiency and signal extraction	energy scale	unfolding
electron channel					
≥ 1 jets	0.151	0.006	0.006	$+0.021$ -0.019	± 0.001
≥ 2 jets	0.028	0.003	0.003	± 0.004	± 0.001
≥ 3 jets	0.0039	0.0009	0.0009	$+0.0007$ -0.0006	$+0.0003$ -0.0001
≥ 4 jets	0.00070	0.00036	0.00036	$+0.00014$ -0.00012	$+0.00005$ -0.00004
muon channel					
≥ 1 jets	0.149	0.005	0.011	$+0.022$ -0.020	± 0.001
≥ 2 jets	0.027	0.003	0.004	± 0.004	± 0.001
≥ 3 jets	0.0042	0.0011	0.0012	$+0.0008$ -0.0006	$+0.0001$ -0.0003
≥ 4 jets	0.00087	0.00050	0.00056	$+0.00017$ -0.00015	$+0.00010$ -0.00001

energy scale, the charge misidentification, and the positive versus negative lepton efficiency difference. The results are compatible with the inclusive charge asymmetry measurement [28].

The charge asymmetry depends on the number of associated jets because the fraction of u (d) quarks contributing to the process is different in each case. The measured values are found to be in good agreement with the predictions based on MADGRAPH with the Z2 tune, while PYTHIA does not describe well the W charge asymmetry, even for events with a single associated jet.

Finally, we test for Berends–Giele scaling [13] and measure its parameters. Events are assigned to exclusive jet multiplicity bins (inclusive for $n \geq 4$), and the corrected yields are fitted with

Table 6: Results for $\sigma(W+ \geq n \text{ jets})/\sigma(W+ \geq (n-1) \text{ jets})$ in the electron and muon channels. A full description of the uncertainties is given in the text.

n jets	$\frac{\sigma(W+\geq n \text{ jets})}{\sigma(W+\geq (n-1) \text{ jets})}$	stat.	stat. + efficiency and signal extraction	energy scale	unfolding
electron channel					
≥ 1 / ≥ 0 jets	0.133	0.002	0.002	$+0.019$ -0.017	± 0.001
≥ 2 / ≥ 1 jets	0.195	0.007	0.007	$+0.002$ -0.001	$+0.012$ -0.001
≥ 3 / ≥ 2 jets	0.125	0.014	0.015	± 0.004	$+0.002$ -0.004
≥ 4 / ≥ 3 jets	0.173	0.046	0.049	$+0.003$ -0.004	$+0.017$ -0.003
muon channel					
≥ 1 / ≥ 0 jets	0.136	0.002	0.007	$+0.019$ -0.017	± 0.001
≥ 2 / ≥ 1 jets	0.190	0.005	0.014	$+0.004$ -0.003	$+0.016$ -0.001
≥ 3 / ≥ 2 jets	0.160	0.011	0.018	$+0.004$ -0.003	$+0.004$ -0.002
≥ 4 / ≥ 3 jets	0.144	0.025	0.037	$+0.002$ -0.003	$+0.001$ -0.043

Table 7: Results for $\sigma(Z+ \geq n \text{ jets})/\sigma(Z+ \geq (n-1) \text{ jets})$ in the electron and muon channels. A full description of the uncertainties is given in the text.

| n jets	$\frac{\sigma(Z+\geq n \text{ jets})}{\sigma(Z+\geq (n-1) \text{ jets})}$	stat.	stat. + efficiency and signal extraction	energy scale	unfolding
electron channel					
≥ 1 / ≥ 0 jets	0.151	0.006	0.006	$+0.021$ -0.019	± 0.001
≥ 2 / ≥ 1 jets	0.185	0.017	0.017	$+0.002$ -0.001	$+0.006$ -0.001
≥ 3 / ≥ 2 jets	0.138	0.030	0.030	± 0.004	$+0.008$ -0.003
≥ 4 / ≥ 3 jets	0.181	0.085	0.085	$+0.003$ -0.004	$+0.014$ -0.021
muon channel					
≥ 1 / ≥ 0 jets	0.149	0.005	0.011	$+0.022$ -0.020	± 0.001
≥ 2 / ≥ 1 jets	0.180	0.016	0.023	± 0.003	$+0.011$ -0.001
≥ 3 / ≥ 2 jets	0.158	0.036	0.043	$+0.002$ -0.001	$+0.001$ -0.017
≥ 4 / ≥ 3 jets	0.207	0.104	0.117	$+0.002$ -0.003	$+0.031$ -0.001
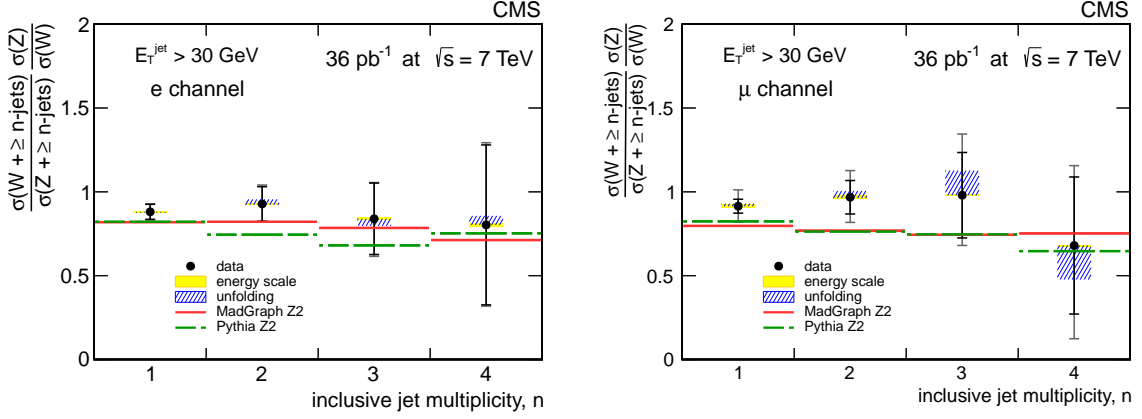
Figure 14: Ratio of the W + jets and Z + jets cross sections for the electron channels (left) and the muon channels (right) as a function of the jet multiplicity. The ratios are normalized to the inclusive W/Z cross section. The expectations from MADGRAPH and PYTHIA simulations, both with the Z2 tune, are shown. These expectations do not differ significantly and they are both in agreement with data. The difference between the expected values of the ratio in electron and muon channels is due to the larger electron acceptance in η. Error bars on data are shown for the statistical and total uncertainties. The uncertainties due to the energy scale and the unfolding procedure are shown as yellow and hatched bands, respectively.

Table 8: W charge asymmetry A_W in the data and in the MADGRAPH and PYTHIA (Z2 tune) simulations for the electron and muon channel. The uncertainties on the simulation values are statistical only.

| n jets	data	MADGRAPH Z2	PYTHIA Z2
electron channel			
≥ 0	$0.217 \pm 0.004 \,(\text{stat.}) \pm 0.006 \,(\text{syst.})$	0.228 ± 0.001	0.216 ± 0.003
≥ 1	$0.179 \pm 0.010 \,(\text{stat.}) \pm 0.007 \,(\text{syst.})$	0.179 ± 0.004	0.267 ± 0.007
≥ 2	$0.16 \pm 0.03 \,(\text{stat.}) \pm 0.01 \,(\text{syst.})$	0.183 ± 0.010	0.281 ± 0.020
≥ 3	$0.17 \pm 0.08 \,(\text{stat.}) \pm 0.06 \,(\text{syst.})$	0.19 ± 0.02	0.33 ± 0.05
muon channel			
≥ 0	$0.223 \pm 0.003 \,(\text{stat.}) \pm 0.010 \,(\text{syst.})$	0.224 ± 0.001	0.237 ± 0.003
≥ 1	$0.175 \pm 0.010 \,(\text{stat.}) \pm 0.011 \,(\text{syst.})$	0.179 ± 0.003	0.222 ± 0.008
≥ 2	$0.18 \pm 0.03 \,(\text{stat.}) \pm 0.02 \,(\text{syst.})$	0.190 ± 0.008	0.273 ± 0.023
≥ 3	$0.22 \pm 0.07 \,(\text{stat.}) \pm 0.02 \,(\text{syst.})$	0.19 ± 0.02	0.26 ± 0.06
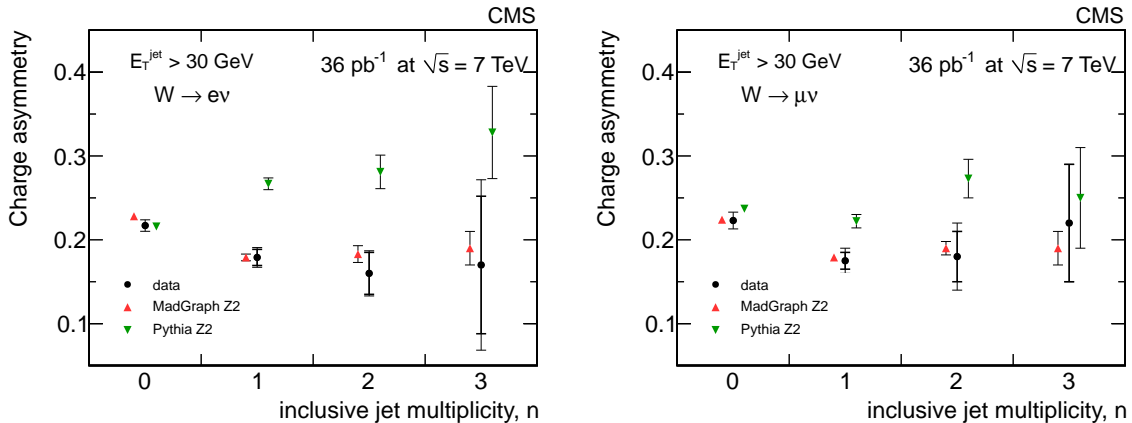
Figure 15: W charge asymmetry A_W versus the inclusive jet multiplicity. Data are compared with predictions from the MADGRAPH and PYTHIA simulations. Error bars on the data points show the statistical and total uncertainties. Error bars on the simulation points correspond to the statistical uncertainty only. Left: electron decay channel, right: muon decay channel.

the assumption that they conform to a scaling function:

$$C_n \equiv \frac{\sigma_n}{\sigma_{n+1}} = \alpha , \tag{1}$$

where $\sigma_n = \sigma(V + \geq n \text{ jets})$, and α is a constant. Previous measurements have shown that the Berends-Giele ratio can be approximately constant [7, 9, 41]. Phase-space effects, however, can violate this simple proportionality. Therefore we introduce a second parameter, β, to allow for a deviation from a constant scaling law:

$$C_n = \alpha + \beta n. \tag{2}$$

Because of the different production kinematics of the $n = 0$ sample, where no reconstructed jets recoil against the vector boson, the scaling expressed in Eq. (2) is not expected to hold, so we do not include the $n = 0$ sample in the fit. The results of the fit for α and β from the W + jets and Z + jets samples are shown in Fig. 16. The values are given in the (α, β) plane and are compared with expectations from MADGRAPH with the Z2 tune for the underlying event description. Generator results are obtained at the particle jet level for events within the lepton and jet acceptance of the selection. The electron and muon expected values differ mostly because of the $\Delta R > 0.3$ requirement between the jets and the leptons, which is applied only in the electron channel. The ellipses correspond to 68% confidence level contours using the statistical uncertainty only. The arrows show the displacement of the central value when varying each indicated parameter by its estimated uncertainty. The fit results are also reported in Tables 9 and 10. The data are in agreement with expectations within one or two standard deviations depending on the channel. Furthermore, the Berends–Giele scaling hypothesis i.e., the relationship shown in Eq. (1), is confirmed to work well up to the production of four jets. The β parameter lies within one standard deviation from zero for the W + jets case and within 0.5 standard deviations for the Z + jets case.

11 Summary

The rate of jet production in association with a W or Z boson was measured in pp collisions at $\sqrt{s} = 7$ TeV. The data were collected with the CMS detector in 2010 and correspond to an integrated luminosity of $36\,\text{pb}^{-1}$. The W + jets and Z + jets samples were reconstructed in the
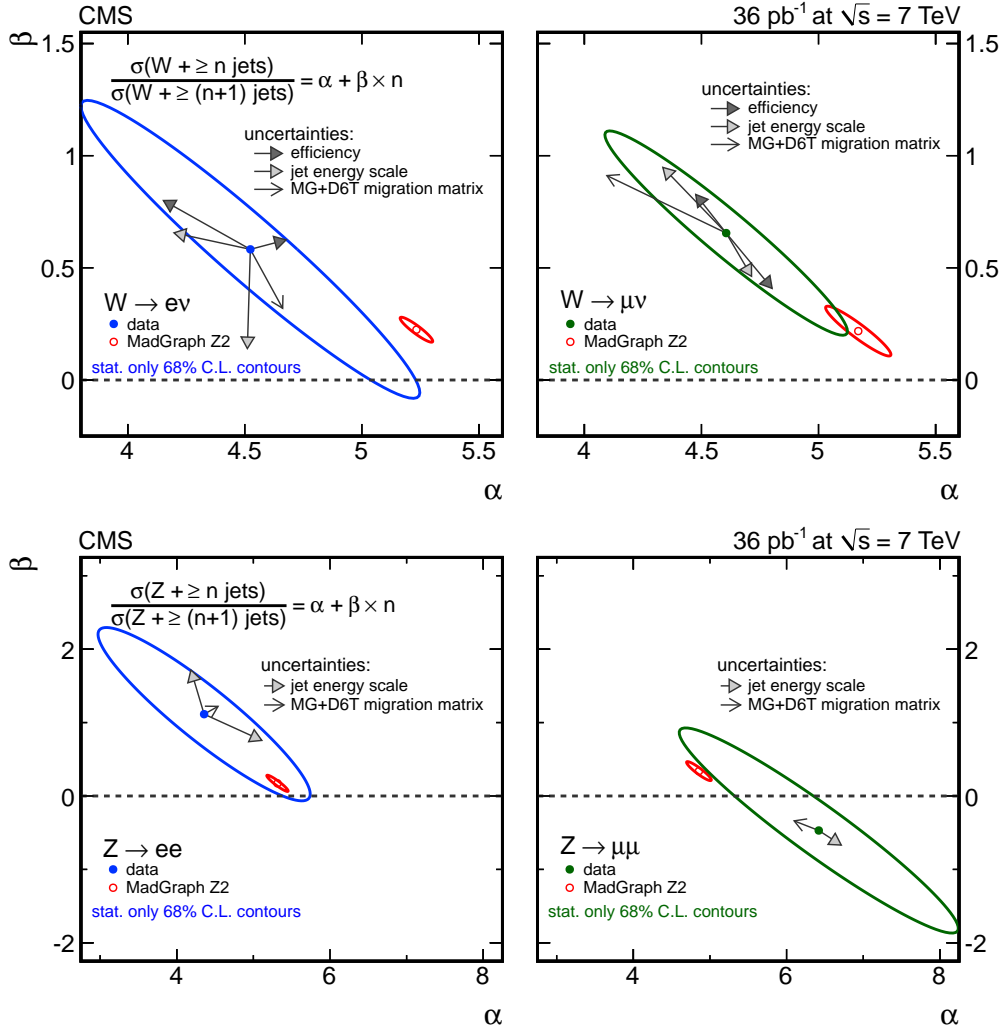
Figure 16: Fit results for the Berends–Giele scaling parameters α and β after pileup subtraction, efficiency corrections, and unfolding of detector resolution effects: (top) W + jets, (bottom) Z + jets, (left) electrons, (right) muons. The data are compared with the expectations from the MADGRAPH simulation with the Z2 tune. The ellipses correspond to 68% confidence level contours considering the statistical uncertainty only, for both data and simulation. The arrows show the displacement of the central value when varying each indicated parameter by its estimated uncertainty. The arrows labelled "MG+D6T migration matrix" correspond to the displacement when MADGRAPH simulation with the D6T tune is used for the unfolding.

Table 9: Results for the Berends–Giele parameters in the electron channel compared with expectations from the MADGRAPH Z2 simulation at the particle level. The prediction uncertainty is statistical only.

		data	stat.	energy scale	efficiency	tune	theory
W	α	4.5	± 0.5	$^{+0.1}_{-0.3}$	$^{+0.2}_{-0.4}$	+0.1	5.20 ± 0.05
	β	0.6	± 0.4	$^{+0.1}_{-0.4}$	$^{+0.2}_{-0.1}$	-0.3	0.20 ± 0.04
Z	α	4.4	± 0.9	$^{+0.8}_{-0.2}$	± 0.05	+0.2	5.3 ± 0.1
	β	1.1	± 0.8	$^{+0.6}_{-0.4}$	± 0.3	+0.1	0.17 ± 0.07

Table 10: Results for the Berends–Giele parameters in the muon channel compared with expectations from the MADGRAPH Z2 simulation at the particle level. The prediction uncertainty is statistical only.

		data	stat.	energy scale	efficiency	tune	theory
W	α	4.6	± 0.3	$^{+0.1}_{-0.3}$	$^{+0.2}_{-0.1}$	-0.5	5.17 ± 0.09
	β	0.7	± 0.3	$^{+0.3}_{-0.2}$	± 0.3	+0.3	0.22 ± 0.07
Z	α	6.4	± 1.2	$^{+0.1}_{-0.3}$	± 0.1	-0.3	4.8 ± 0.1
	β	-0.5	± 0.9	$^{+0.1}_{-0.2}$	± 0.2	+0.1	0.34 ± 0.09

electron and muon decay channels. The measurement was performed using particle-flow jets with $E_\mathrm{T} > 30$ GeV and clustered with the anti-k_T algorithm with a size parameter $R = 0.5$.

The E_T spectra agree well with the predictions from simulations based on MADGRAPH interfaced with PYTHIA, and using the Z2 tune for the underlying event description.

Detector resolution effects were unfolded to extract the exclusive jet multiplicity distributions and to measure the ratios of the normalized inclusive rates $\sigma(\mathrm{V}+ \geq n\ \mathrm{jets})/\sigma(\mathrm{V})$. The ratio of the W + jets to Z + jets cross sections, $[\sigma(\mathrm{W}+ \geq n\ \mathrm{jets})/\sigma(\mathrm{Z}+ \geq n\ \mathrm{jets})]/[\sigma(\mathrm{Z})/\sigma(\mathrm{W})]$, and the W charge asymmetry, A_W, were also measured as functions of the jet multiplicity. Finally, a quantitative test of Berends–Giele scaling, parametrized as a function of two parameters determined by a fit, was performed.

All results are in agreement with the predictions of the MADGRAPH generator, using matrix-element calculations for final states with jets, matched with PYTHIA parton shower. In contrast, the simulation based on parton showers alone fails to describe the jet rates for more than one jet, and the W charge asymmetry, even in the case of only one jet.

Acknowledgements

References

[1] H. Ita, Z. Bern, L. Dixon et al., "Precise Predictions for Z + 4 Jets at Hadron Colliders", (2011). `arXiv:1108.2229v2`.

[2] C. F. Berger et al., "Precise Predictions for W + 4-Jet Production at the Large Hadron Collider", *Phys. Rev. Lett.* **106** (2011) 092001. `doi:10.1103/PhysRevLett.106.092001`.

[3] C. F. Berger et al., "Next-to-leading order QCD predictions for W + 3-jet distributions at hadron colliders", *Phys. Rev. D* **80** (2009) 074036. `doi:10.1103/PhysRevD.80.074036`.

[4] R. K. Ellis, K. Melnikov, and G. Zanderighi, "W + 3 jet production at the Tevatron", *Phys. Rev. D* **80** (2009) 094002. `doi:10.1103/PhysRevD.80.094002`.

[5] C. F. Berger et al., "Next-to-leading order QCD predictions for Z, γ^* + 3-jet distributions at the Tevatron", *Phys. Rev. D* **82** (2010) 074002. `doi:10.1103/PhysRevD.82.074002`.

[6] C.-H. Kom and W. Stirling, "Charge asymmetry in W + jets production at the LHC", *Eur. Phys. J. C* **69** (2010) 67. `doi:10.1140/epjc/s10052-010-1353-z`.

[7] CDF Collaboration Collaboration, "Measurement of the cross section for W-boson production in association with jets in p$\overline{\text{p}}$ collisions at $\sqrt{s} = 1.96$ TeV", *Phys. Rev. D* **77** (2008) 011108. `doi:10.1103/PhysRevD.77.011108`.

[8] CDF Collaboration Collaboration, "Measurement of Inclusive Jet Cross Sections in $Z/\gamma^*(\to e^+e^-)+$ jets Production in p$\overline{\text{p}}$ Collisions at $\sqrt{s} = 1.96$ TeV", *Phys. Rev. Lett.* **100** (2008) 102001. `doi:10.1103/PhysRevLett.100.102001`.

[9] D0 Collaboration, "Measurements of inclusive W+jets production rates as a function of jet transverse momentum in p$\overline{\text{p}}$ collisions at $\sqrt{s} = 1.96$ TeV", (2011). `arXiv:1106.1457v1`.

[10] D0 Collaboration, "Measurements of differential cross sections of Z/γ^*+jets+X events in proton anti-proton collisions at $\sqrt{s} = 1.96$ TeV", *Phys. Lett. B* **678** (2009) 45. `doi:10.1016/j.physletb.2009.05.058`.

[11] ATLAS Collaboration, "Measurement of the production cross section for W-bosons in association with jets in pp collisions at sqrt(s) = 7 TeV with the ATLAS detector", *Phys. Lett. B* **698** (2011) 325. `doi:10.1016/j.physletb.2011.03.012`.

[12] CMS Collaboration, "Absolute luminosity normalization", CMS Detector Performance Summary DP-2011-002, (2011).

[13] F. A. Berends et al., "Multi-jet production in W, Z events at p anti-p colliders", *Phys. Lett. B* **224** (1989) 237. `doi:10.1016/0370-2693(89)91081-2`.

[14] CMS Collaboration, "The CMS experiment at the CERN LHC", *JINST* **3** (2008) S08004. `doi:10.1088/1748-0221/3/08/S08004`.

[15] F. Maltoni and T. Stelzer, "MadEvent: Automatic event generation with MadGraph", *JHEP* **02** (2003) 027. `doi:10.1088/1126-6708/2003/02/027`.

[16] T. Sjöstrand, S. Mrenna, and P. Z. Skands, "PYTHIA 6.4 Physics and Manual", *JHEP* **05** (2006) 026. `doi:10.1088/1126-6708/2006/05/026`.

[17] J. Pumplin et al., "New generation of parton distributions with uncertainties from global QCD analysis", *JHEP* **07** (2002) 012. `doi:10.1088/1126-6708/2002/07/012`.

[18] K. Melnikov and F. Petriello, "Electroweak gauge boson production at hadron colliders through $\mathcal{O}(\alpha_s^2)$", *Phys. Rev. D* **74** (2006) 114017. `doi:10.1103/PhysRevD.74.114017`.

[19] J. M. Campbell, R. Frederex, F. Maltoni et al., "Next-to-Leading-Order Predictions for t-Channel Single-Top Production at Hadron Colliders", *Phys. Rev. Lett.* **102** (2009) 182003. `doi:10.1103/PhysRevLett.102.182003`.

[20] R. Kleiss and W. J. Stirling, "Top quark production at hadron colliders: some useful formulae", *Z. Phys. C* **40** (1988) 419. `doi:10.1007/BF01548856`.

[21] GEANT4 Collaboration, "GEANT4: A simulation toolkit", *Nucl. Instrum. Meth. A* **506** (2003) 250. `doi:10.1016/S0168-9002(03)01368-8`.

[22] J. Allison et al., "Geant4 developments and applications", *IEEE Trans. Nucl. Sci.* **53** (2006) 270. `doi:10.1109/TNS.2006.869826`.

[23] CMS Collaboration, "Measurement of the Underlying Event Activity at the LHC with $\sqrt{s} = 7$ TeV and Comparison with $\sqrt{s} = 0.9$ TeV", (2011). `arXiv:1107.0330v1`. Submitted to JHEP.

[24] R. Field, "Early LHC Underlying Event Data - Findings and Surprisses", (2010). `arXiv:1010.3558`.

[25] P. Z. Skands, "Tuning Monte Carlo Generators: The Perugia Tunes", *Phys. Rev. D* **82** (2010) 074018. `doi:10.1103/PhysRevD.82.074018`.

[26] CMS Collaboration, "Measurements of Inclusive W and Z Cross Sections in pp Collisions at $\sqrt{s}$=7 TeV", *JHEP* **01** (2011) 080. `doi:10.1007/JHEP01(2011)080`.

[27] CMS Collaboration, "Commissioning of the Particle-Flow Reconstruction in Minimum-Bias and Jet Events from pp Collisions at 7 TeV", CMS Physics Analysis Summary CMS-PAS-PFT-10-002, (2010).

[28] CMS Collaboration, "Measurement of the lepton charge asymmetry in inclusive W production in pp collisions at $\sqrt{s} = 7$ TeV", *JHEP* **04** (2011) 050. `doi:10.1007/JHEP04(2011)050`.

[29] W. Adam et al., "Reconstruction of Electrons with the Gaussian-Sum Filter in the CMS Tracker at the LHC", CMS Note 2005/001, (2005).

[30] M. Cacciari, G.P. Salam and G. Soyez, "The anti-k_t jet clustering algorithm", *JHEP* **04** (2008) 063. `doi:10.1088/1126-6708/2008/04/063`.

[31] CMS Collaboration, "Determination of Jet Energy Calibration and Transverse Momentum Resolution in CMS", (2011). `arXiv:1107.4277`. Submitted to JINST.

[32] CMS Collaboration, "Identification and Filtering of Uncharacteristic Noise in the CMS Hadron Calorimeter", *JINST* **05** (2010) T03014. `doi:10.1088/1748-0221/5/03/T03014`.

[33] M. Cacciari and G. Salam, "Pileup subtraction using jet areas", *Phys. Lett. B* **659** (2008) 119. `doi:10.1016/j.physletb.2007.09.077`.

[34] M. Cacciari, G. Salam, and G. Soyez, "The catchment area of jets", *JHEP* **04** (2008) 005. `doi:10.1088/1126-6708/2008/04/005`.

[35] CMS Collaboration, "Performance of b-jet identification in CMS", CMS Physics Analysis Summary CMS-PAS-BTV-11-001, (2011).

[36] CMS Collaboration, "Measurement of the charge ratio of atmospheric muons with the CMS detector", *Phys. Lett. B* **692** (2010) 83. `doi:10.1016/j.physletb.2010.07.033`.

[37] A. Hocker and V. Kartvelishvili, "SVD Approach to Data Unfolding", *Nucl. Instrum. Meth. A* **372** (1996) 469. `doi:10.1016/0168-9002(95)01478-0`.

[38] G. D'Agostini, "A multidimensional unfolding method based on Bayes' theorem", *Nucl. Instrum. Meth. A* **362** (1995) 487. `doi:10.1016/0168-9002(95)00274-X`.

[39] T. Adye, "Unfolding algorithms and tests using RooUnfold", (2011). `arXiv:1105.1160`.

[40] CMS Collaboration, "Jet Energy Resolution in CMS at $\sqrt{s} = 7$ TeV", CMS Physics Analysis Summary CMS-PAS-JME-10-014, (2010).

[41] D0 Collaboration, "$t\bar{t}$ production cross section in p$\bar{\text{p}}$ collisions at $\sqrt{s} = 1.8$ TeV", *Phys. Rev. D* **67** (2003) 012004. `doi:10.1103/PhysRevD.67.012004`.

A   The CMS Collaboration

Yerevan Physics Institute, Yerevan, Armenia
S. Chatrchyan, V. Khachatryan, A.M. Sirunyan, A. Tumasyan

Institut für Hochenergiephysik der OeAW, Wien, Austria
W. Adam, T. Bergauer, M. Dragicevic, J. Erö, C. Fabjan, M. Friedl, R. Frühwirth, V.M. Ghete, J. Hammer[1], S. Hänsel, M. Hoch, N. Hörmann, J. Hrubec, M. Jeitler, W. Kiesenhofer, M. Krammer, D. Liko, I. Mikulec, M. Pernicka, B. Rahbaran, H. Rohringer, R. Schöfbeck, J. Strauss, A. Taurok, F. Teischinger, C. Trauner, P. Wagner, W. Waltenberger, G. Walzel, E. Widl, C.-E. Wulz

National Centre for Particle and High Energy Physics, Minsk, Belarus
V. Mossolov, N. Shumeiko, J. Suarez Gonzalez

Universiteit Antwerpen, Antwerpen, Belgium
S. Bansal, L. Benucci, E.A. De Wolf, X. Janssen, S. Luyckx, T. Maes, L. Mucibello, S. Ochesanu, B. Roland, R. Rougny, M. Selvaggi, H. Van Haevermaet, P. Van Mechelen, N. Van Remortel

Vrije Universiteit Brussel, Brussel, Belgium
F. Blekman, S. Blyweert, J. D'Hondt, R. Gonzalez Suarez, A. Kalogeropoulos, M. Maes, A. Olbrechts, W. Van Doninck, P. Van Mulders, G.P. Van Onsem, I. Villella

Université Libre de Bruxelles, Bruxelles, Belgium
O. Charaf, B. Clerbaux, G. De Lentdecker, V. Dero, A.P.R. Gay, G.H. Hammad, T. Hreus, P.E. Marage, A. Raval, L. Thomas, G. Vander Marcken, C. Vander Velde, P. Vanlaer

Ghent University, Ghent, Belgium
V. Adler, A. Cimmino, S. Costantini, M. Grunewald, B. Klein, J. Lellouch, A. Marinov, J. Mccartin, D. Ryckbosch, F. Thyssen, M. Tytgat, L. Vanelderen, P. Verwilligen, S. Walsh, N. Zaganidis

Université Catholique de Louvain, Louvain-la-Neuve, Belgium
S. Basegmez, G. Bruno, J. Caudron, L. Ceard, E. Cortina Gil, J. De Favereau De Jeneret, C. Delaere, D. Favart, A. Giammanco, G. Grégoire, J. Hollar, V. Lemaitre, J. Liao, O. Militaru, C. Nuttens, S. Ovyn, D. Pagano, A. Pin, K. Piotrzkowski, N. Schul

Université de Mons, Mons, Belgium
N. Beliy, T. Caebergs, E. Daubie

Centro Brasileiro de Pesquisas Fisicas, Rio de Janeiro, Brazil
G.A. Alves, D. De Jesus Damiao, M.E. Pol, M.H.G. Souza

Universidade do Estado do Rio de Janeiro, Rio de Janeiro, Brazil
W.L. Aldá Júnior, W. Carvalho, E.M. Da Costa, C. De Oliveira Martins, S. Fonseca De Souza, D. Matos Figueiredo, L. Mundim, H. Nogima, V. Oguri, W.L. Prado Da Silva, A. Santoro, S.M. Silva Do Amaral, A. Sznajder

Instituto de Fisica Teorica, Universidade Estadual Paulista, Sao Paulo, Brazil
T.S. Anjos[2], C.A. Bernardes[2], F.A. Dias[3], T.R. Fernandez Perez Tomei, E. M. Gregores[2], C. Lagana, F. Marinho, P.G. Mercadante[2], S.F. Novaes, Sandra S. Padula

Institute for Nuclear Research and Nuclear Energy, Sofia, Bulgaria
N. Darmenov[1], V. Genchev[1], P. Iaydjiev[1], S. Piperov, M. Rodozov, S. Stoykova, G. Sultanov, V. Tcholakov, R. Trayanov, M. Vutova

University of Sofia, Sofia, Bulgaria
A. Dimitrov, R. Hadjiiska, A. Karadzhinova, V. Kozhuharov, L. Litov, M. Mateev, B. Pavlov, P. Petkov

Institute of High Energy Physics, Beijing, China
J.G. Bian, G.M. Chen, H.S. Chen, C.H. Jiang, D. Liang, S. Liang, X. Meng, J. Tao, J. Wang, J. Wang, X. Wang, Z. Wang, H. Xiao, M. Xu, J. Zang, Z. Zhang

State Key Lab. of Nucl. Phys. and Tech., Peking University, Beijing, China
Y. Ban, S. Guo, Y. Guo, W. Li, Y. Mao, S.J. Qian, H. Teng, B. Zhu, W. Zou

Universidad de Los Andes, Bogota, Colombia
A. Cabrera, B. Gomez Moreno, A.A. Ocampo Rios, A.F. Osorio Oliveros, J.C. Sanabria

Technical University of Split, Split, Croatia
N. Godinovic, D. Lelas, K. Lelas, R. Plestina[4], D. Polic, I. Puljak

University of Split, Split, Croatia
Z. Antunovic, M. Dzelalija, M. Kovac

Institute Rudjer Boskovic, Zagreb, Croatia
V. Brigljevic, S. Duric, K. Kadija, J. Luetic, S. Morovic

University of Cyprus, Nicosia, Cyprus
A. Attikis, M. Galanti, J. Mousa, C. Nicolaou, F. Ptochos, P.A. Razis

Charles University, Prague, Czech Republic
M. Finger, M. Finger Jr.

Academy of Scientific Research and Technology of the Arab Republic of Egypt, Egyptian Network of High Energy Physics, Cairo, Egypt
Y. Assran[5], A. Ellithi Kamel[6], S. Khalil[7], M.A. Mahmoud[8], A. Radi[9]

National Institute of Chemical Physics and Biophysics, Tallinn, Estonia
A. Hektor, M. Kadastik, M. Müntel, M. Raidal, L. Rebane, A. Tiko

Department of Physics, University of Helsinki, Helsinki, Finland
V. Azzolini, P. Eerola, G. Fedi, M. Voutilainen

Helsinki Institute of Physics, Helsinki, Finland
S. Czellar, J. Härkönen, A. Heikkinen, V. Karimäki, R. Kinnunen, M.J. Kortelainen, T. Lampén, K. Lassila-Perini, S. Lehti, T. Lindén, P. Luukka, T. Mäenpää, E. Tuominen, J. Tuominiemi, E. Tuovinen, D. Ungaro, L. Wendland

Lappeenranta University of Technology, Lappeenranta, Finland
K. Banzuzi, A. Karjalainen, A. Korpela, T. Tuuva

Laboratoire d'Annecy-le-Vieux de Physique des Particules, IN2P3-CNRS, Annecy-le-Vieux, France
D. Sillou

DSM/IRFU, CEA/Saclay, Gif-sur-Yvette, France
M. Besancon, S. Choudhury, M. Dejardin, D. Denegri, B. Fabbro, J.L. Faure, F. Ferri, S. Ganjour, F.X. Gentit, A. Givernaud, P. Gras, G. Hamel de Monchenault, P. Jarry, E. Locci, J. Malcles, M. Marionneau, L. Millischer, J. Rander, A. Rosowsky, I. Shreyber, M. Titov, P. Verrecchia

Laboratoire Leprince-Ringuet, Ecole Polytechnique, IN2P3-CNRS, Palaiseau, France
S. Baffioni, F. Beaudette, L. Benhabib, L. Bianchini, M. Bluj[10], C. Broutin, P. Busson, C. Charlot, T. Dahms, L. Dobrzynski, S. Elgammal, R. Granier de Cassagnac, M. Haguenauer, P. Miné, C. Mironov, C. Ochando, P. Paganini, D. Sabes, R. Salerno, Y. Sirois, C. Thiebaux, C. Veelken, A. Zabi

Institut Pluridisciplinaire Hubert Curien, Université de Strasbourg, Université de Haute Alsace Mulhouse, CNRS/IN2P3, Strasbourg, France
J.-L. Agram[11], J. Andrea, D. Bloch, D. Bodin, J.-M. Brom, M. Cardaci, E.C. Chabert, C. Collard, E. Conte[11], F. Drouhin[11], C. Ferro, J.-C. Fontaine[11], D. Gelé, U. Goerlach, S. Greder, P. Juillot, M. Karim[11], A.-C. Le Bihan, Y. Mikami, P. Van Hove

Centre de Calcul de l'Institut National de Physique Nucleaire et de Physique des Particules (IN2P3), Villeurbanne, France
F. Fassi, D. Mercier

Université de Lyon, Université Claude Bernard Lyon 1, CNRS-IN2P3, Institut de Physique Nucléaire de Lyon, Villeurbanne, France
C. Baty, S. Beauceron, N. Beaupere, M. Bedjidian, O. Bondu, G. Boudoul, D. Boumediene, H. Brun, J. Chasserat, R. Chierici, D. Contardo, P. Depasse, H. El Mamouni, J. Fay, S. Gascon, B. Ille, T. Kurca, T. Le Grand, M. Lethuillier, L. Mirabito, S. Perries, V. Sordini, S. Tosi, Y. Tschudi, P. Verdier, S. Viret

Institute of High Energy Physics and Informatization, Tbilisi State University, Tbilisi, Georgia
D. Lomidze

RWTH Aachen University, I. Physikalisches Institut, Aachen, Germany
G. Anagnostou, S. Beranek, M. Edelhoff, L. Feld, N. Heracleous, O. Hindrichs, R. Jussen, K. Klein, J. Merz, N. Mohr, A. Ostapchuk, A. Perieanu, F. Raupach, J. Sammet, S. Schael, D. Sprenger, H. Weber, M. Weber, B. Wittmer, V. Zhukov[12]

RWTH Aachen University, III. Physikalisches Institut A, Aachen, Germany
M. Ata, E. Dietz-Laursonn, M. Erdmann, T. Hebbeker, C. Heidemann, A. Hinzmann, K. Hoepfner, T. Klimkovich, D. Klingebiel, P. Kreuzer, D. Lanske[†], J. Lingemann, C. Magass, M. Merschmeyer, A. Meyer, P. Papacz, H. Pieta, H. Reithler, S.A. Schmitz, L. Sonnenschein, J. Steggemann, D. Teyssier

RWTH Aachen University, III. Physikalisches Institut B, Aachen, Germany
M. Bontenackels, V. Cherepanov, M. Davids, G. Flügge, H. Geenen, M. Giffels, W. Haj Ahmad, F. Hoehle, B. Kargoll, T. Kress, Y. Kuessel, A. Linn, A. Nowack, L. Perchalla, O. Pooth, J. Rennefeld, P. Sauerland, A. Stahl, D. Tornier, M.H. Zoeller

Deutsches Elektronen-Synchrotron, Hamburg, Germany
M. Aldaya Martin, W. Behrenhoff, U. Behrens, M. Bergholz[13], A. Bethani, K. Borras, A. Cakir, A. Campbell, E. Castro, D. Dammann, G. Eckerlin, D. Eckstein, A. Flossdorf, G. Flucke, A. Geiser, J. Hauk, H. Jung[1], M. Kasemann, P. Katsas, C. Kleinwort, H. Kluge, A. Knutsson, M. Krämer, D. Krücker, E. Kuznetsova, W. Lange, W. Lohmann[13], R. Mankel, M. Marienfeld, I.-A. Melzer-Pellmann, A.B. Meyer, J. Mnich, A. Mussgiller, J. Olzem, A. Petrukhin, D. Pitzl, A. Raspereza, M. Rosin, R. Schmidt[13], T. Schoerner-Sadenius, N. Sen, A. Spiridonov, M. Stein, J. Tomaszewska, R. Walsh, C. Wissing

University of Hamburg, Hamburg, Germany
C. Autermann, V. Blobel, S. Bobrovskyi, J. Draeger, H. Enderle, U. Gebbert, M. Görner,

T. Hermanns, K. Kaschube, G. Kaussen, H. Kirschenmann, R. Klanner, J. Lange, B. Mura, S. Naumann-Emme, F. Nowak, N. Pietsch, C. Sander, H. Schettler, P. Schleper, E. Schlieckau, M. Schröder, T. Schum, H. Stadie, G. Steinbrück, J. Thomsen

Institut für Experimentelle Kernphysik, Karlsruhe, Germany
C. Barth, J. Bauer, J. Berger, V. Buege, T. Chwalek, W. De Boer, A. Dierlamm, G. Dirkes, M. Feindt, J. Gruschke, C. Hackstein, F. Hartmann, M. Heinrich, H. Held, K.H. Hoffmann, S. Honc, I. Katkov[12], J.R. Komaragiri, T. Kuhr, D. Martschei, S. Mueller, Th. Müller, M. Niegel, O. Oberst, A. Oehler, J. Ott, T. Peiffer, G. Quast, K. Rabbertz, F. Ratnikov, N. Ratnikova, M. Renz, S. Röcker, C. Saout, A. Scheurer, P. Schieferdecker, F.-P. Schilling, M. Schmanau, G. Schott, H.J. Simonis, F.M. Stober, D. Troendle, J. Wagner-Kuhr, T. Weiler, M. Zeise, E.B. Ziebarth

Institute of Nuclear Physics "Demokritos", Aghia Paraskevi, Greece
G. Daskalakis, T. Geralis, S. Kesisoglou, A. Kyriakis, D. Loukas, I. Manolakos, A. Markou, C. Markou, C. Mavrommatis, E. Ntomari, E. Petrakou

University of Athens, Athens, Greece
L. Gouskos, T.J. Mertzimekis, A. Panagiotou, N. Saoulidou, E. Stiliaris

University of Ioánnina, Ioánnina, Greece
I. Evangelou, C. Foudas[1], P. Kokkas, N. Manthos, I. Papadopoulos, V. Patras, F.A. Triantis

KFKI Research Institute for Particle and Nuclear Physics, Budapest, Hungary
A. Aranyi, G. Bencze, L. Boldizsar, C. Hajdu[1], P. Hidas, D. Horvath[14], A. Kapusi, K. Krajczar[15], F. Sikler[1], G.I. Veres[15], G. Vesztergombi[15]

Institute of Nuclear Research ATOMKI, Debrecen, Hungary
N. Beni, J. Molnar, J. Palinkas, Z. Szillasi, V. Veszpremi

University of Debrecen, Debrecen, Hungary
P. Raics, Z.L. Trocsanyi, B. Ujvari

Panjab University, Chandigarh, India
S.B. Beri, V. Bhatnagar, N. Dhingra, R. Gupta, M. Jindal, M. Kaur, J.M. Kohli, M.Z. Mehta, N. Nishu, L.K. Saini, A. Sharma, A.P. Singh, J. Singh, S.P. Singh

University of Delhi, Delhi, India
S. Ahuja, B.C. Choudhary, P. Gupta, A. Kumar, A. Kumar, S. Malhotra, M. Naimuddin, K. Ranjan, R.K. Shivpuri

Saha Institute of Nuclear Physics, Kolkata, India
S. Banerjee, S. Bhattacharya, S. Dutta, B. Gomber, S. Jain, S. Jain, R. Khurana, S. Sarkar

Bhabha Atomic Research Centre, Mumbai, India
R.K. Choudhury, D. Dutta, S. Kailas, V. Kumar, P. Mehta, A.K. Mohanty[1], L.M. Pant, P. Shukla

Tata Institute of Fundamental Research - EHEP, Mumbai, India
T. Aziz, M. Guchait[16], A. Gurtu, M. Maity[17], D. Majumder, G. Majumder, T. Mathew, K. Mazumdar, G.B. Mohanty, A. Saha, K. Sudhakar, N. Wickramage

Tata Institute of Fundamental Research - HECR, Mumbai, India
S. Banerjee, S. Dugad, N.K. Mondal

Institute for Research and Fundamental Sciences (IPM), Tehran, Iran
H. Arfaei, H. Bakhshiansohi[18], S.M. Etesami[19], A. Fahim[18], M. Hashemi, H. Hesari, A. Jafari[18],

M. Khakzad, A. Mohammadi[20], M. Mohammadi Najafabadi, S. Paktinat Mehdiabadi, B. Safarzadeh, M. Zeinali[19]

INFN Sezione di Bari [a], Università di Bari [b], Politecnico di Bari [c], Bari, Italy
M. Abbrescia[a,b], L. Barbone[a,b], C. Calabria[a,b], A. Colaleo[a], D. Creanza[a,c], N. De Filippis[a,c,1], M. De Palma[a,b], L. Fiore[a], G. Iaselli[a,c], L. Lusito[a,b], G. Maggi[a,c], M. Maggi[a], N. Manna[a,b], B. Marangelli[a,b], S. My[a,c], S. Nuzzo[a,b], N. Pacifico[a,b], G.A. Pierro[a], A. Pompili[a,b], G. Pugliese[a,c], F. Romano[a,c], G. Roselli[a,b], G. Selvaggi[a,b], L. Silvestris[a], R. Trentadue[a], S. Tupputi[a,b], G. Zito[a]

INFN Sezione di Bologna [a], Università di Bologna [b], Bologna, Italy
G. Abbiendi[a], A.C. Benvenuti[a], D. Bonacorsi[a], S. Braibant-Giacomelli[a,b], L. Brigliadori[a], P. Capiluppi[a,b], A. Castro[a,b], F.R. Cavallo[a], M. Cuffiani[a,b], G.M. Dallavalle[a], F. Fabbri[a], A. Fanfani[a,b], D. Fasanella[a,1], P. Giacomelli[a], M. Giunta[a], C. Grandi[a], S. Marcellini[a], G. Masetti[b], M. Meneghelli[a,b], A. Montanari[a], F.L. Navarria[a,b], F. Odorici[a], A. Perrotta[a], F. Primavera[a], A.M. Rossi[a,b], T. Rovelli[a,b], G. Siroli[a,b], R. Travaglini[a,b]

INFN Sezione di Catania [a], Università di Catania [b], Catania, Italy
S. Albergo[a,b], G. Cappello[a,b], M. Chiorboli[a,b], S. Costa[a,b], R. Potenza[a,b], A. Tricomi[a,b], C. Tuve[a,b]

INFN Sezione di Firenze [a], Università di Firenze [b], Firenze, Italy
G. Barbagli[a], V. Ciulli[a,b], C. Civinini[a], R. D'Alessandro[a,b], E. Focardi[a,b], S. Frosali[a,b], E. Gallo[a], S. Gonzi[a,b], P. Lenzi[a,b], M. Meschini[a], S. Paoletti[a], G. Sguazzoni[a], A. Tropiano[a,1]

INFN Laboratori Nazionali di Frascati, Frascati, Italy
L. Benussi, S. Bianco, S. Colafranceschi[21], F. Fabbri, D. Piccolo

INFN Sezione di Genova, Genova, Italy
P. Fabbricatore, R. Musenich

INFN Sezione di Milano-Bicocca [a], Università di Milano-Bicocca [b], Milano, Italy
A. Benaglia[a,b,1], F. De Guio[a,b], L. Di Matteo[a,b], S. Gennai[1], A. Ghezzi[a,b], S. Malvezzi[a], A. Martelli[a,b], A. Massironi[a,b,1], D. Menasce[a], L. Moroni[a], M. Paganoni[a,b], D. Pedrini[a], S. Ragazzi[a,b], N. Redaelli[a], S. Sala[a], T. Tabarelli de Fatis[a,b]

INFN Sezione di Napoli [a], Università di Napoli "Federico II" [b], Napoli, Italy
S. Buontempo[a], C.A. Carrillo Montoya[a,1], N. Cavallo[a,22], A. De Cosa[a,b], F. Fabozzi[a,22], A.O.M. Iorio[a,1], L. Lista[a], M. Merola[a,b], P. Paolucci[a]

INFN Sezione di Padova [a], Università di Padova [b], Università di Trento (Trento) [c], Padova, Italy
P. Azzi[a], N. Bacchetta[a,1], P. Bellan[a,b], D. Bisello[a,b], A. Branca[a], R. Carlin[a,b], P. Checchia[a], T. Dorigo[a], U. Dosselli[a], F. Fanzago[a], F. Gasparini[a,b], U. Gasparini[a,b], A. Gozzelino, S. Lacaprara[a,23], I. Lazzizzera[a,c], M. Margoni[a,b], M. Mazzucato[a], A.T. Meneguzzo[a,b], M. Nespolo[a,1], L. Perrozzi[a], N. Pozzobon[a,b], P. Ronchese[a,b], F. Simonetto[a,b], E. Torassa[a], M. Tosi[a,b,1], S. Vanini[a,b], P. Zotto[a,b], G. Zumerle[a,b]

INFN Sezione di Pavia [a], Università di Pavia [b], Pavia, Italy
P. Baesso[a,b], U. Berzano[a], S.P. Ratti[a,b], C. Riccardi[a,b], P. Torre[a,b], P. Vitulo[a,b], C. Viviani[a,b]

INFN Sezione di Perugia [a], Università di Perugia [b], Perugia, Italy
M. Biasini[a,b], G.M. Bilei[a], B. Caponeri[a,b], L. Fanò[a,b], P. Lariccia[a,b], A. Lucaroni[a,b,1], G. Mantovani[a,b], M. Menichelli[a], A. Nappi[a,b], F. Romeo[a,b], A. Santocchia[a,b], S. Taroni[a,b,1], M. Valdata[a,b]

INFN Sezione di Pisa *ᵃ*, **Università di Pisa** *ᵇ*, **Scuola Normale Superiore di Pisa** *ᶜ*, **Pisa, Italy**
P. Azzurri^{a,c}, G. Bagliesi^a, J. Bernardini^{a,b}, T. Boccali^a, G. Broccolo^{a,c}, R. Castaldi^a, R.T. D'Agnolo^{a,c}, R. Dell'Orso^a, F. Fiori^{a,b}, L. Foà^{a,c}, A. Giassi^a, A. Kraan^a, F. Ligabue^{a,c}, T. Lomtadze^a, L. Martini^{a,24}, A. Messineo^{a,b}, F. Palla^a, F. Palmonari, G. Segneri^a, A.T. Serban^a, P. Spagnolo^a, R. Tenchini^a, G. Tonelli^{a,b,1}, A. Venturi^{a,1}, P.G. Verdini^a

INFN Sezione di Roma *ᵃ*, **Università di Roma "La Sapienza"** *ᵇ*, **Roma, Italy**
L. Barone^{a,b}, F. Cavallari^a, D. Del Re^{a,b,1}, E. Di Marco^{a,b}, M. Diemoz^a, D. Franci^{a,b}, M. Grassi^{a,1}, E. Longo^{a,b}, P. Meridiani, F. Micheli, S. Nourbakhsh^a, G. Organtini^{a,b}, F. Pandolfi^{a,b}, R. Paramatti^a, S. Rahatlou^{a,b}, M. Sigamani^a

INFN Sezione di Torino *ᵃ*, **Università di Torino** *ᵇ*, **Università del Piemonte Orientale (Novara)** *ᶜ*, **Torino, Italy**
N. Amapane^{a,b}, R. Arcidiacono^{a,c}, S. Argiro^{a,b}, M. Arneodo^{a,c}, C. Biino^a, C. Botta^{a,b}, N. Cartiglia^a, R. Castello^{a,b}, M. Costa^{a,b}, N. Demaria^a, A. Graziano^{a,b}, C. Mariotti^a, S. Maselli^a, E. Migliore^{a,b}, V. Monaco^{a,b}, M. Musich^a, M.M. Obertino^{a,c}, N. Pastrone^a, M. Pelliccioni^{a,b}, A. Potenza^{a,b}, A. Romero^{a,b}, M. Ruspa^{a,c}, R. Sacchi^{a,b}, V. Sola^{a,b}, A. Solano^{a,b}, A. Staiano^a, A. Vilela Pereira^a

INFN Sezione di Trieste *ᵃ*, **Università di Trieste** *ᵇ*, **Trieste, Italy**
S. Belforte^a, F. Cossutti^a, G. Della Ricca^{a,b}, B. Gobbo^a, M. Marone^{a,b}, D. Montanino^{a,b}, A. Penzo^a, A. Schizzi^{a,b}

Kangwon National University, Chunchon, Korea
S.G. Heo, S.K. Nam

Kyungpook National University, Daegu, Korea
S. Chang, J. Chung, D.H. Kim, G.N. Kim, J.E. Kim, D.J. Kong, H. Park, S.R. Ro, D.C. Son, T. Son

Chonnam National University, Institute for Universe and Elementary Particles, Kwangju, Korea
J.Y. Kim, Zero J. Kim, S. Song

Konkuk University, Seoul, Korea
H.Y. Jo

Korea University, Seoul, Korea
S. Choi, D. Gyun, B. Hong, M. Jo, H. Kim, J.H. Kim, T.J. Kim, K.S. Lee, D.H. Moon, S.K. Park, E. Seo, K.S. Sim

University of Seoul, Seoul, Korea
M. Choi, S. Kang, H. Kim, C. Park, I.C. Park, S. Park, G. Ryu

Sungkyunkwan University, Suwon, Korea
Y. Cho, Y. Choi, Y.K. Choi, J. Goh, M.S. Kim, B. Lee, J. Lee, S. Lee, H. Seo, I. Yu

Vilnius University, Vilnius, Lithuania
M.J. Bilinskas, I. Grigelionis, M. Janulis, D. Martisiute, P. Petrov, M. Polujanskas, T. Sabonis

Centro de Investigacion y de Estudios Avanzados del IPN, Mexico City, Mexico
H. Castilla-Valdez, E. De La Cruz-Burelo, I. Heredia-de La Cruz, R. Lopez-Fernandez, R. Magaña Villalba, J. Martínez-Ortega, A. Sánchez-Hernández, L.M. Villasenor-Cendejas

Universidad Iberoamericana, Mexico City, Mexico
S. Carrillo Moreno, F. Vazquez Valencia

Benemerita Universidad Autonoma de Puebla, Puebla, Mexico
H.A. Salazar Ibarguen

Universidad Autónoma de San Luis Potosí, San Luis Potosí, Mexico
E. Casimiro Linares, A. Morelos Pineda, M.A. Reyes-Santos

University of Auckland, Auckland, New Zealand
D. Krofcheck, J. Tam

University of Canterbury, Christchurch, New Zealand
P.H. Butler, R. Doesburg, H. Silverwood

National Centre for Physics, Quaid-I-Azam University, Islamabad, Pakistan
M. Ahmad, I. Ahmed, M.H. Ansari, M.I. Asghar, H.R. Hoorani, S. Khalid, W.A. Khan, T. Khurshid, S. Qazi, M.A. Shah, M. Shoaib

Institute of Experimental Physics, Faculty of Physics, University of Warsaw, Warsaw, Poland
G. Brona, M. Cwiok, W. Dominik, K. Doroba, A. Kalinowski, M. Konecki, J. Krolikowski

Soltan Institute for Nuclear Studies, Warsaw, Poland
T. Frueboes, R. Gokieli, M. Górski, M. Kazana, K. Nawrocki, K. Romanowska-Rybinska, M. Szleper, G. Wrochna, P. Zalewski

Laboratório de Instrumentação e Física Experimental de Partículas, Lisboa, Portugal
N. Almeida, P. Bargassa, A. David, P. Faccioli, P.G. Ferreira Parracho, M. Gallinaro[1], P. Musella, A. Nayak, J. Pela[1], P.Q. Ribeiro, J. Seixas, J. Varela

Joint Institute for Nuclear Research, Dubna, Russia
S. Afanasiev, I. Belotelov, P. Bunin, M. Gavrilenko, I. Golutvin, A. Kamenev, V. Karjavin, G. Kozlov, A. Lanev, P. Moisenz, V. Palichik, V. Perelygin, S. Shmatov, V. Smirnov, A. Volodko, A. Zarubin

Petersburg Nuclear Physics Institute, Gatchina (St Petersburg), Russia
V. Golovtsov, Y. Ivanov, V. Kim, P. Levchenko, V. Murzin, V. Oreshkin, I. Smirnov, V. Sulimov, L. Uvarov, S. Vavilov, A. Vorobyev, An. Vorobyev

Institute for Nuclear Research, Moscow, Russia
Yu. Andreev, A. Dermenev, S. Gninenko, N. Golubev, M. Kirsanov, N. Krasnikov, V. Matveev, A. Pashenkov, A. Toropin, S. Troitsky

Institute for Theoretical and Experimental Physics, Moscow, Russia
V. Epshteyn, M. Erofeeva, V. Gavrilov, V. Kaftanov[†], M. Kossov[1], A. Krokhotin, N. Lychkovskaya, V. Popov, G. Safronov, S. Semenov, V. Stolin, E. Vlasov, A. Zhokin

Moscow State University, Moscow, Russia
A. Belyaev, E. Boos, M. Dubinin[3], L. Dudko, A. Ershov, A. Gribushin, O. Kodolova, I. Lokhtin, A. Markina, S. Obraztsov, M. Perfilov, S. Petrushanko, L. Sarycheva, V. Savrin, A. Snigirev

P.N. Lebedev Physical Institute, Moscow, Russia
V. Andreev, M. Azarkin, I. Dremin, M. Kirakosyan, A. Leonidov, G. Mesyats, S.V. Rusakov, A. Vinogradov

State Research Center of Russian Federation, Institute for High Energy Physics, Protvino, Russia
I. Azhgirey, I. Bayshev, S. Bitioukov, V. Grishin[1], V. Kachanov, D. Konstantinov, A. Korablev,

V. Krychkine, V. Petrov, R. Ryutin, A. Sobol, L. Tourtchanovitch, S. Troshin, N. Tyurin, A. Uzunian, A. Volkov

University of Belgrade, Faculty of Physics and Vinca Institute of Nuclear Sciences, Belgrade, Serbia
P. Adzic[25], M. Djordjevic, D. Krpic[25], J. Milosevic

Centro de Investigaciones Energéticas Medioambientales y Tecnológicas (CIEMAT), Madrid, Spain
M. Aguilar-Benitez, J. Alcaraz Maestre, P. Arce, C. Battilana, E. Calvo, M. Cerrada, M. Chamizo Llatas, N. Colino, B. De La Cruz, A. Delgado Peris, C. Diez Pardos, D. Domínguez Vázquez, C. Fernandez Bedoya, J.P. Fernández Ramos, A. Ferrando, J. Flix, M.C. Fouz, P. Garcia-Abia, O. Gonzalez Lopez, S. Goy Lopez, J.M. Hernandez, M.I. Josa, G. Merino, J. Puerta Pelayo, I. Redondo, L. Romero, J. Santaolalla, M.S. Soares, C. Willmott

Universidad Autónoma de Madrid, Madrid, Spain
C. Albajar, G. Codispoti, J.F. de Trocóniz

Universidad de Oviedo, Oviedo, Spain
J. Cuevas, J. Fernandez Menendez, S. Folgueras, I. Gonzalez Caballero, L. Lloret Iglesias, J.M. Vizan Garcia

Instituto de Física de Cantabria (IFCA), CSIC-Universidad de Cantabria, Santander, Spain
J.A. Brochero Cifuentes, I.J. Cabrillo, A. Calderon, S.H. Chuang, J. Duarte Campderros, M. Felcini[26], M. Fernandez, G. Gomez, J. Gonzalez Sanchez, C. Jorda, P. Lobelle Pardo, A. Lopez Virto, J. Marco, R. Marco, C. Martinez Rivero, F. Matorras, F.J. Munoz Sanchez, J. Piedra Gomez[27], T. Rodrigo, A.Y. Rodríguez-Marrero, A. Ruiz-Jimeno, L. Scodellaro, M. Sobron Sanudo, I. Vila, R. Vilar Cortabitarte

CERN, European Organization for Nuclear Research, Geneva, Switzerland
D. Abbaneo, E. Auffray, G. Auzinger, P. Baillon, A.H. Ball, D. Barney, A.J. Bell[28], D. Benedetti, C. Bernet[4], W. Bialas, P. Bloch, A. Bocci, S. Bolognesi, M. Bona, H. Breuker, K. Bunkowski, T. Camporesi, G. Cerminara, T. Christiansen, J.A. Coarasa Perez, B. Curé, D. D'Enterria, A. De Roeck, S. Di Guida, N. Dupont-Sagorin, A. Elliott-Peisert, B. Frisch, W. Funk, A. Gaddi, G. Georgiou, H. Gerwig, D. Gigi, K. Gill, D. Giordano, F. Glege, R. Gomez-Reino Garrido, M. Gouzevitch, P. Govoni, S. Gowdy, R. Guida, L. Guiducci, M. Hansen, C. Hartl, J. Harvey, J. Hegeman, B. Hegner, H.F. Hoffmann, V. Innocente, P. Janot, K. Kaadze, E. Karavakis, P. Lecoq, C. Lourenço, T. Mäki, M. Malberti, L. Malgeri, M. Mannelli, L. Masetti, A. Maurisset, F. Meijers, S. Mersi, E. Meschi, R. Moser, M.U. Mozer, M. Mulders, E. Nesvold, M. Nguyen, T. Orimoto, L. Orsini, E. Palencia Cortezon, E. Perez, A. Petrilli, A. Pfeiffer, M. Pierini, M. Pimiä, D. Piparo, G. Polese, L. Quertenmont, A. Racz, W. Reece, J. Rodrigues Antunes, G. Rolandi[29], T. Rommerskirchen, C. Rovelli[30], M. Rovere, H. Sakulin, C. Schäfer, C. Schwick, I. Segoni, A. Sharma, P. Siegrist, P. Silva, M. Simon, P. Sphicas[31], D. Spiga, M. Spiropulu[3], M. Stoye, A. Tsirou, P. Vichoudis, H.K. Wöhri, S.D. Worm, W.D. Zeuner

Paul Scherrer Institut, Villigen, Switzerland
W. Bertl, K. Deiters, W. Erdmann, K. Gabathuler, R. Horisberger, Q. Ingram, H.C. Kaestli, S. König, D. Kotlinski, U. Langenegger, F. Meier, D. Renker, T. Rohe, J. Sibille[32]

Institute for Particle Physics, ETH Zurich, Zurich, Switzerland
L. Bäni, P. Bortignon, L. Caminada[33], B. Casal, N. Chanon, Z. Chen, S. Cittolin, G. Dissertori, M. Dittmar, J. Eugster, K. Freudenreich, C. Grab, W. Hintz, P. Lecomte, W. Lustermann, C. Marchica[33], P. Martinez Ruiz del Arbol, P. Milenovic[34], F. Moortgat, C. Nägeli[33], P. Nef,

F. Nessi-Tedaldi, L. Pape, F. Pauss, T. Punz, A. Rizzi, F.J. Ronga, M. Rossini, L. Sala, A.K. Sanchez, M.-C. Sawley, A. Starodumov[35], B. Stieger, M. Takahashi, L. Tauscher[†], A. Thea, K. Theofilatos, D. Treille, C. Urscheler, R. Wallny, M. Weber, L. Wehrli, J. Weng

Universität Zürich, Zurich, Switzerland
E. Aguilo, C. Amsler, V. Chiochia, S. De Visscher, C. Favaro, M. Ivova Rikova, A. Jaeger, B. Millan Mejias, P. Otiougova, P. Robmann, A. Schmidt, H. Snoek

National Central University, Chung-Li, Taiwan
Y.H. Chang, K.H. Chen, C.M. Kuo, S.W. Li, W. Lin, Z.K. Liu, Y.J. Lu, D. Mekterovic, R. Volpe, S.S. Yu

National Taiwan University (NTU), Taipei, Taiwan
P. Bartalini, P. Chang, Y.H. Chang, Y.W. Chang, Y. Chao, K.F. Chen, W.-S. Hou, Y. Hsiung, K.Y. Kao, Y.J. Lei, R.-S. Lu, J.G. Shiu, Y.M. Tzeng, X. Wan, M. Wang

Cukurova University, Adana, Turkey
A. Adiguzel, M.N. Bakirci[36], S. Cerci[37], C. Dozen, I. Dumanoglu, E. Eskut, S. Girgis, G. Gokbulut, I. Hos, E.E. Kangal, A. Kayis Topaksu, G. Onengut, K. Ozdemir, S. Ozturk[38], A. Polatoz, K. Sogut[39], D. Sunar Cerci[37], B. Tali[37], H. Topakli[36], D. Uzun, L.N. Vergili, M. Vergili

Middle East Technical University, Physics Department, Ankara, Turkey
I.V. Akin, T. Aliev, B. Bilin, S. Bilmis, M. Deniz, H. Gamsizkan, A.M. Guler, K. Ocalan, A. Ozpineci, M. Serin, R. Sever, U.E. Surat, M. Yalvac, E. Yildirim, M. Zeyrek

Bogazici University, Istanbul, Turkey
M. Deliomeroglu, D. Demir[40], E. Gülmez, B. Isildak, M. Kaya[41], O. Kaya[41], M. Özbek, S. Ozkorucuklu[42], N. Sonmez[43]

National Scientific Center, Kharkov Institute of Physics and Technology, Kharkov, Ukraine
L. Levchuk

University of Bristol, Bristol, United Kingdom
F. Bostock, J.J. Brooke, T.L. Cheng, E. Clement, D. Cussans, R. Frazier, J. Goldstein, M. Grimes, D. Hartley, G.P. Heath, H.F. Heath, L. Kreczko, S. Metson, D.M. Newbold[44], K. Nirunpong, A. Poll, S. Senkin, V.J. Smith

Rutherford Appleton Laboratory, Didcot, United Kingdom
L. Basso[45], K.W. Bell, A. Belyaev[45], C. Brew, R.M. Brown, B. Camanzi, D.J.A. Cockerill, J.A. Coughlan, K. Harder, S. Harper, J. Jackson, B.W. Kennedy, E. Olaiya, D. Petyt, B.C. Radburn-Smith, C.H. Shepherd-Themistocleous, I.R. Tomalin, W.J. Womersley

Imperial College, London, United Kingdom
R. Bainbridge, G. Ball, J. Ballin, R. Beuselinck, O. Buchmuller, D. Colling, N. Cripps, M. Cutajar, G. Davies, M. Della Negra, W. Ferguson, J. Fulcher, D. Futyan, A. Gilbert, A. Guneratne Bryer, G. Hall, Z. Hatherell, J. Hays, G. Iles, M. Jarvis, G. Karapostoli, L. Lyons, B.C. MacEvoy, A.-M. Magnan, J. Marrouche, B. Mathias, R. Nandi, J. Nash, A. Nikitenko[35], A. Papageorgiou, M. Pesaresi, K. Petridis, M. Pioppi[46], D.M. Raymond, S. Rogerson, N. Rompotis, A. Rose, M.J. Ryan, C. Seez, P. Sharp, A. Sparrow, A. Tapper, S. Tourneur, M. Vazquez Acosta, T. Virdee, S. Wakefield, N. Wardle, D. Wardrope, T. Whyntie

Brunel University, Uxbridge, United Kingdom
M. Barrett, M. Chadwick, J.E. Cole, P.R. Hobson, A. Khan, P. Kyberd, D. Leslie, W. Martin, I.D. Reid, L. Teodorescu

Baylor University, Waco, USA
K. Hatakeyama, H. Liu

The University of Alabama, Tuscaloosa, USA
C. Henderson

Boston University, Boston, USA
T. Bose, E. Carrera Jarrin, C. Fantasia, A. Heister, J. St. John, P. Lawson, D. Lazic, J. Rohlf, D. Sperka, L. Sulak

Brown University, Providence, USA
A. Avetisyan, S. Bhattacharya, J.P. Chou, D. Cutts, A. Ferapontov, U. Heintz, S. Jabeen, G. Kukartsev, G. Landsberg, M. Luk, M. Narain, D. Nguyen, M. Segala, T. Sinthuprasith, T. Speer, K.V. Tsang

University of California, Davis, Davis, USA
R. Breedon, G. Breto, M. Calderon De La Barca Sanchez, S. Chauhan, M. Chertok, J. Conway, R. Conway, P.T. Cox, J. Dolen, R. Erbacher, R. Houtz, W. Ko, A. Kopecky, R. Lander, H. Liu, O. Mall, S. Maruyama, T. Miceli, M. Nikolic, D. Pellett, J. Robles, B. Rutherford, S. Salur, T. Schwarz, M. Searle, J. Smith, M. Squires, M. Tripathi, R. Vasquez Sierra

University of California, Los Angeles, Los Angeles, USA
V. Andreev, K. Arisaka, D. Cline, R. Cousins, A. Deisher, J. Duris, S. Erhan, C. Farrell, J. Hauser, M. Ignatenko, C. Jarvis, C. Plager, G. Rakness, P. Schlein[†], J. Tucker, V. Valuev

University of California, Riverside, Riverside, USA
J. Babb, R. Clare, J. Ellison, J.W. Gary, F. Giordano, G. Hanson, G.Y. Jeng, S.C. Kao, H. Liu, O.R. Long, A. Luthra, H. Nguyen, S. Paramesvaran, B.C. Shen[†], J. Sturdy, S. Sumowidagdo, R. Wilken, S. Wimpenny

University of California, San Diego, La Jolla, USA
W. Andrews, J.G. Branson, G.B. Cerati, D. Evans, F. Golf, A. Holzner, R. Kelley, M. Lebourgeois, J. Letts, B. Mangano, S. Padhi, C. Palmer, G. Petrucciani, H. Pi, M. Pieri, R. Ranieri, M. Sani, V. Sharma, S. Simon, E. Sudano, M. Tadel, Y. Tu, A. Vartak, S. Wasserbaech[47], F. Würthwein, A. Yagil, J. Yoo

University of California, Santa Barbara, Santa Barbara, USA
D. Barge, R. Bellan, C. Campagnari, M. D'Alfonso, T. Danielson, K. Flowers, P. Geffert, J. Incandela, C. Justus, P. Kalavase, S.A. Koay, D. Kovalskyi[1], V. Krutelyov, S. Lowette, N. Mccoll, S.D. Mullin, V. Pavlunin, F. Rebassoo, J. Ribnik, J. Richman, R. Rossin, D. Stuart, W. To, J.R. Vlimant, C. West

California Institute of Technology, Pasadena, USA
A. Apresyan, A. Bornheim, J. Bunn, Y. Chen, J. Duarte, M. Gataullin, Y. Ma, A. Mott, H.B. Newman, C. Rogan, K. Shin, V. Timciuc, P. Traczyk, J. Veverka, R. Wilkinson, Y. Yang, R.Y. Zhu

Carnegie Mellon University, Pittsburgh, USA
B. Akgun, R. Carroll, T. Ferguson, Y. Iiyama, D.W. Jang, S.Y. Jun, Y.F. Liu, M. Paulini, J. Russ, H. Vogel, I. Vorobiev

University of Colorado at Boulder, Boulder, USA
J.P. Cumalat, M.E. Dinardo, B.R. Drell, C.J. Edelmaier, W.T. Ford, A. Gaz, B. Heyburn, E. Luiggi Lopez, U. Nauenberg, J.G. Smith, K. Stenson, K.A. Ulmer, S.R. Wagner, S.L. Zang

Cornell University, Ithaca, USA
L. Agostino, J. Alexander, A. Chatterjee, N. Eggert, L.K. Gibbons, B. Heltsley, K. Henriksson, W. Hopkins, A. Khukhunaishvili, B. Kreis, Y. Liu, G. Nicolas Kaufman, J.R. Patterson, D. Puigh, A. Ryd, M. Saelim, E. Salvati, X. Shi, W. Sun, W.D. Teo, J. Thom, J. Thompson, J. Vaughan, Y. Weng, L. Winstrom, P. Wittich

Fairfield University, Fairfield, USA
A. Biselli, G. Cirino, D. Winn

Fermi National Accelerator Laboratory, Batavia, USA
S. Abdullin, M. Albrow, J. Anderson, G. Apollinari, M. Atac, J.A. Bakken, L.A.T. Bauerdick, A. Beretvas, J. Berryhill, P.C. Bhat, I. Bloch, K. Burkett, J.N. Butler, V. Chetluru, H.W.K. Cheung, F. Chlebana, S. Cihangir, W. Cooper, D.P. Eartly, V.D. Elvira, S. Esen, I. Fisk, J. Freeman, Y. Gao, E. Gottschalk, D. Green, O. Gutsche, J. Hanlon, R.M. Harris, J. Hirschauer, B. Hooberman, H. Jensen, S. Jindariani, M. Johnson, U. Joshi, B. Klima, K. Kousouris, S. Kunori, S. Kwan, C. Leonidopoulos, P. Limon, D. Lincoln, R. Lipton, J. Lykken, K. Maeshima, J.M. Marraffino, D. Mason, P. McBride, T. Miao, K. Mishra, S. Mrenna, Y. Musienko[48], C. Newman-Holmes, V. O'Dell, J. Pivarski, R. Pordes, O. Prokofyev, E. Sexton-Kennedy, S. Sharma, W.J. Spalding, L. Spiegel, P. Tan, L. Taylor, S. Tkaczyk, L. Uplegger, E.W. Vaandering, R. Vidal, J. Whitmore, W. Wu, F. Yang, F. Yumiceva, J.C. Yun

University of Florida, Gainesville, USA
D. Acosta, P. Avery, D. Bourilkov, M. Chen, S. Das, M. De Gruttola, G.P. Di Giovanni, D. Dobur, A. Drozdetskiy, R.D. Field, M. Fisher, Y. Fu, I.K. Furic, J. Gartner, S. Goldberg, J. Hugon, B. Kim, J. Konigsberg, A. Korytov, A. Kropivnitskaya, T. Kypreos, J.F. Low, K. Matchev, G. Mitselmakher, L. Muniz, P. Myeonghun, C. Prescott, R. Remington, A. Rinkevicius, M. Schmitt, B. Scurlock, P. Sellers, N. Skhirtladze, M. Snowball, D. Wang, J. Yelton, M. Zakaria

Florida International University, Miami, USA
V. Gaultney, L.M. Lebolo, S. Linn, P. Markowitz, G. Martinez, J.L. Rodriguez

Florida State University, Tallahassee, USA
T. Adams, A. Askew, J. Bochenek, J. Chen, B. Diamond, S.V. Gleyzer, J. Haas, S. Hagopian, V. Hagopian, M. Jenkins, K.F. Johnson, H. Prosper, S. Sekmen, V. Veeraraghavan

Florida Institute of Technology, Melbourne, USA
M.M. Baarmand, B. Dorney, M. Hohlmann, H. Kalakhety, I. Vodopiyanov

University of Illinois at Chicago (UIC), Chicago, USA
M.R. Adams, I.M. Anghel, L. Apanasevich, Y. Bai, V.E. Bazterra, R.R. Betts, J. Callner, R. Cavanaugh, C. Dragoiu, L. Gauthier, C.E. Gerber, D.J. Hofman, S. Khalatyan, G.J. Kunde[49], F. Lacroix, M. Malek, C. O'Brien, C. Silkworth, C. Silvestre, A. Smoron, D. Strom, N. Varelas

The University of Iowa, Iowa City, USA
U. Akgun, E.A. Albayrak, B. Bilki, W. Clarida, F. Duru, C.K. Lae, E. McCliment, J.-P. Merlo, H. Mermerkaya[50], A. Mestvirishvili, A. Moeller, J. Nachtman, C.R. Newsom, E. Norbeck, J. Olson, Y. Onel, F. Ozok, S. Sen, J. Wetzel, T. Yetkin, K. Yi

Johns Hopkins University, Baltimore, USA
B.A. Barnett, B. Blumenfeld, A. Bonato, C. Eskew, D. Fehling, G. Giurgiu, A.V. Gritsan, Z.J. Guo, G. Hu, P. Maksimovic, S. Rappoccio, M. Swartz, N.V. Tran, A. Whitbeck

The University of Kansas, Lawrence, USA

P. Baringer, A. Bean, G. Benelli, O. Grachov, R.P. Kenny Iii, M. Murray, D. Noonan, S. Sanders, R. Stringer, J.S. Wood, V. Zhukova

Kansas State University, Manhattan, USA
A.F. Barfuss, T. Bolton, I. Chakaberia, A. Ivanov, S. Khalil, M. Makouski, Y. Maravin, S. Shrestha, I. Svintradze

Lawrence Livermore National Laboratory, Livermore, USA
J. Gronberg, D. Lange, D. Wright

University of Maryland, College Park, USA
A. Baden, M. Boutemeur, S.C. Eno, D. Ferencek, J.A. Gomez, N.J. Hadley, R.G. Kellogg, M. Kirn, Y. Lu, A.C. Mignerey, K. Rossato, P. Rumerio, F. Santanastasio, A. Skuja, J. Temple, M.B. Tonjes, S.C. Tonwar, E. Twedt

Massachusetts Institute of Technology, Cambridge, USA
B. Alver, G. Bauer, J. Bendavid, W. Busza, E. Butz, I.A. Cali, M. Chan, V. Dutta, P. Everaerts, G. Gomez Ceballos, M. Goncharov, K.A. Hahn, P. Harris, Y. Kim, M. Klute, Y.-J. Lee, W. Li, C. Loizides, P.D. Luckey, T. Ma, S. Nahn, C. Paus, D. Ralph, C. Roland, G. Roland, M. Rudolph, G.S.F. Stephans, F. Stöckli, K. Sumorok, K. Sung, D. Velicanu, E.A. Wenger, R. Wolf, B. Wyslouch, S. Xie, M. Yang, Y. Yilmaz, A.S. Yoon, M. Zanetti

University of Minnesota, Minneapolis, USA
S.I. Cooper, P. Cushman, B. Dahmes, A. De Benedetti, G. Franzoni, A. Gude, J. Haupt, K. Klapoetke, Y. Kubota, J. Mans, N. Pastika, V. Rekovic, R. Rusack, M. Sasseville, A. Singovsky, N. Tambe, J. Turkewitz

University of Mississippi, University, USA
L.M. Cremaldi, R. Godang, R. Kroeger, L. Perera, R. Rahmat, D.A. Sanders, D. Summers

University of Nebraska-Lincoln, Lincoln, USA
K. Bloom, S. Bose, J. Butt, D.R. Claes, A. Dominguez, M. Eads, P. Jindal, J. Keller, T. Kelly, I. Kravchenko, J. Lazo-Flores, H. Malbouisson, S. Malik, G.R. Snow

State University of New York at Buffalo, Buffalo, USA
U. Baur, A. Godshalk, I. Iashvili, S. Jain, A. Kharchilava, A. Kumar, K. Smith, Z. Wan

Northeastern University, Boston, USA
G. Alverson, E. Barberis, D. Baumgartel, O. Boeriu, M. Chasco, S. Reucroft, J. Swain, D. Trocino, D. Wood, J. Zhang

Northwestern University, Evanston, USA
A. Anastassov, A. Kubik, N. Mucia, N. Odell, R.A. Ofierzynski, B. Pollack, A. Pozdnyakov, M. Schmitt, S. Stoynev, M. Velasco, S. Won

University of Notre Dame, Notre Dame, USA
L. Antonelli, D. Berry, A. Brinkerhoff, M. Hildreth, C. Jessop, D.J. Karmgard, J. Kolb, T. Kolberg, K. Lannon, W. Luo, S. Lynch, N. Marinelli, D.M. Morse, T. Pearson, R. Ruchti, J. Slaunwhite, N. Valls, M. Wayne, J. Ziegler

The Ohio State University, Columbus, USA
B. Bylsma, L.S. Durkin, J. Gu, C. Hill, P. Killewald, K. Kotov, T.Y. Ling, M. Rodenburg, C. Vuosalo, G. Williams

Princeton University, Princeton, USA
N. Adam, E. Berry, P. Elmer, D. Gerbaudo, V. Halyo, P. Hebda, A. Hunt, E. Laird, D. Lopes

Pegna, D. Marlow, T. Medvedeva, M. Mooney, J. Olsen, P. Piroué, X. Quan, B. Safdi, H. Saka, D. Stickland, C. Tully, J.S. Werner, A. Zuranski

University of Puerto Rico, Mayaguez, USA
J.G. Acosta, X.T. Huang, A. Lopez, H. Mendez, S. Oliveros, J.E. Ramirez Vargas, A. Zatserklyaniy

Purdue University, West Lafayette, USA
E. Alagoz, V.E. Barnes, G. Bolla, L. Borrello, D. Bortoletto, M. De Mattia, A. Everett, A.F. Garfinkel, L. Gutay, Z. Hu, M. Jones, O. Koybasi, M. Kress, A.T. Laasanen, N. Leonardo, C. Liu, V. Maroussov, P. Merkel, D.H. Miller, N. Neumeister, I. Shipsey, D. Silvers, A. Svyatkovskiy, M. Vidal Marono, H.D. Yoo, J. Zablocki, Y. Zheng

Purdue University Calumet, Hammond, USA
S. Guragain, N. Parashar

Rice University, Houston, USA
A. Adair, C. Boulahouache, K.M. Ecklund, F.J.M. Geurts, B.P. Padley, R. Redjimi, J. Roberts, J. Zabel

University of Rochester, Rochester, USA
B. Betchart, A. Bodek, Y.S. Chung, R. Covarelli, P. de Barbaro, R. Demina, Y. Eshaq, H. Flacher, A. Garcia-Bellido, P. Goldenzweig, Y. Gotra, J. Han, A. Harel, D.C. Miner, G. Petrillo, W. Sakumoto, D. Vishnevskiy, M. Zielinski

The Rockefeller University, New York, USA
A. Bhatti, R. Ciesielski, L. Demortier, K. Goulianos, G. Lungu, S. Malik, C. Mesropian

Rutgers, the State University of New Jersey, Piscataway, USA
S. Arora, O. Atramentov, A. Barker, C. Contreras-Campana, E. Contreras-Campana, D. Duggan, Y. Gershtein, R. Gray, E. Halkiadakis, D. Hidas, D. Hits, A. Lath, S. Panwalkar, R. Patel, A. Richards, K. Rose, S. Schnetzer, S. Somalwar, R. Stone, S. Thomas

University of Tennessee, Knoxville, USA
G. Cerizza, M. Hollingsworth, S. Spanier, Z.C. Yang, A. York

Texas A&M University, College Station, USA
R. Eusebi, W. Flanagan, J. Gilmore, A. Gurrola, T. Kamon[51], V. Khotilovich, R. Montalvo, I. Osipenkov, Y. Pakhotin, A. Perloff, A. Safonov, S. Sengupta, I. Suarez, A. Tatarinov, D. Toback

Texas Tech University, Lubbock, USA
N. Akchurin, C. Bardak, J. Damgov, P.R. Dudero, C. Jeong, K. Kovitanggoon, S.W. Lee, T. Libeiro, P. Mane, Y. Roh, A. Sill, I. Volobouev, R. Wigmans, E. Yazgan

Vanderbilt University, Nashville, USA
E. Appelt, E. Brownson, D. Engh, C. Florez, W. Gabella, M. Issah, W. Johns, C. Johnston, P. Kurt, C. Maguire, A. Melo, P. Sheldon, B. Snook, S. Tuo, J. Velkovska

University of Virginia, Charlottesville, USA
M.W. Arenton, M. Balazs, S. Boutle, B. Cox, B. Francis, S. Goadhouse, J. Goodell, R. Hirosky, A. Ledovskoy, C. Lin, C. Neu, J. Wood, R. Yohay

Wayne State University, Detroit, USA
S. Gollapinni, R. Harr, P.E. Karchin, C. Kottachchi Kankanamge Don, P. Lamichhane, M. Mattson, C. Milstène, A. Sakharov

University of Wisconsin, Madison, USA
M. Anderson, M. Bachtis, D. Belknap, J.N. Bellinger, D. Carlsmith, M. Cepeda, S. Dasu, J. Efron,
E. Friis, L. Gray, K.S. Grogg, M. Grothe, R. Hall-Wilton, M. Herndon, A. Hervé, P. Klabbers,
J. Klukas, A. Lanaro, C. Lazaridis, J. Leonard, R. Loveless, A. Mohapatra, I. Ojalvo, W. Parker,
I. Ross, A. Savin, W.H. Smith, J. Swanson, M. Weinberg

†: Deceased
1: Also at CERN, European Organization for Nuclear Research, Geneva, Switzerland
2: Also at Universidade Federal do ABC, Santo Andre, Brazil
3: Also at California Institute of Technology, Pasadena, USA
4: Also at Laboratoire Leprince-Ringuet, Ecole Polytechnique, IN2P3-CNRS, Palaiseau, France
5: Also at Suez Canal University, Suez, Egypt
6: Also at Cairo University, Cairo, Egypt
7: Also at British University, Cairo, Egypt
8: Also at Fayoum University, El-Fayoum, Egypt
9: Also at Ain Shams University, Cairo, Egypt
10: Also at Soltan Institute for Nuclear Studies, Warsaw, Poland
11: Also at Université de Haute-Alsace, Mulhouse, France
12: Also at Moscow State University, Moscow, Russia
13: Also at Brandenburg University of Technology, Cottbus, Germany
14: Also at Institute of Nuclear Research ATOMKI, Debrecen, Hungary
15: Also at Eötvös Loránd University, Budapest, Hungary
16: Also at Tata Institute of Fundamental Research - HECR, Mumbai, India
17: Also at University of Visva-Bharati, Santiniketan, India
18: Also at Sharif University of Technology, Tehran, Iran
19: Also at Isfahan University of Technology, Isfahan, Iran
20: Also at Shiraz University, Shiraz, Iran
21: Also at Facoltà Ingegneria Università di Roma, Roma, Italy
22: Also at Università della Basilicata, Potenza, Italy
23: Also at Laboratori Nazionali di Legnaro dell' INFN, Legnaro, Italy
24: Also at Università degli studi di Siena, Siena, Italy
25: Also at Faculty of Physics of University of Belgrade, Belgrade, Serbia
26: Also at University of California, Los Angeles, Los Angeles, USA
27: Also at University of Florida, Gainesville, USA
28: Also at Université de Genève, Geneva, Switzerland
29: Also at Scuola Normale e Sezione dell' INFN, Pisa, Italy
30: Also at INFN Sezione di Roma; Università di Roma "La Sapienza", Roma, Italy
31: Also at University of Athens, Athens, Greece
32: Also at The University of Kansas, Lawrence, USA
33: Also at Paul Scherrer Institut, Villigen, Switzerland
34: Also at University of Belgrade, Faculty of Physics and Vinca Institute of Nuclear Sciences,
Belgrade, Serbia
35: Also at Institute for Theoretical and Experimental Physics, Moscow, Russia
36: Also at Gaziosmanpasa University, Tokat, Turkey
37: Also at Adiyaman University, Adiyaman, Turkey
38: Also at The University of Iowa, Iowa City, USA
39: Also at Mersin University, Mersin, Turkey
40: Also at Izmir Institute of Technology, Izmir, Turkey
41: Also at Kafkas University, Kars, Turkey
42: Also at Suleyman Demirel University, Isparta, Turkey

43: Also at Ege University, Izmir, Turkey

44: Also at Rutherford Appleton Laboratory, Didcot, United Kingdom

45: Also at School of Physics and Astronomy, University of Southampton, Southampton, United Kingdom

46: Also at INFN Sezione di Perugia; Università di Perugia, Perugia, Italy

47: Also at Utah Valley University, Orem, USA

48: Also at Institute for Nuclear Research, Moscow, Russia

49: Also at Los Alamos National Laboratory, Los Alamos, USA

50: Also at Erzincan University, Erzincan, Turkey

51: Also at Kyungpook National University, Daegu, Korea